

# DEBRIS-FLOW MOBILIZATION FROM LANDSLIDES<sup>1</sup>

*Richard M. Iverson*

US Geological Survey, 5400 MacArthur Blvd., Vancouver, Washington 98661;  
e-mail: riverson@usgs.gov

*Mark E. Reid*

US Geological Survey, 345 Middlefield Rd., Menlo Park, California 94025

*Richard G. LaHusen*

US Geological Survey, 5400 MacArthur Blvd., Vancouver, Washington 98661

KEY WORDS: debris flow, mudflow, initiation, hillslope, soil, mechanics, pore pressure

---

## ABSTRACT

Field observations, laboratory experiments, and theoretical analyses indicate that landslides mobilize to form debris flows by three processes: (a) widespread Coulomb failure within a sloping soil, rock, or sediment mass, (b) partial or complete liquefaction of the mass by high pore-fluid pressures, and (c) conversion of landslide translational energy to internal vibrational energy (i.e. granular temperature). These processes can operate independently, but in many circumstances they appear to operate simultaneously and synergistically. Early work on debris-flow mobilization described a similar interplay of processes but relied on mechanical models in which debris behavior was assumed to be fixed and governed by a Bingham or Bagnold rheology. In contrast, this review emphasizes models in which debris behavior evolves in response to changing pore pressures and granular temperatures. One-dimensional infinite-slope models provide insight by quantifying how pore pressures and granular temperatures can influence the transition from Coulomb failure to liquefaction. Analyses of multidimensional experiments reveal complications ignored in one-dimensional models and demonstrate that debris-flow mobilization may occur by at least two distinct modes in the field.

---

<sup>1</sup>The US government has the right to retain a nonexclusive, royalty-free license in and to any copyright covering this paper.

## INTRODUCTION

Debris flows occur when masses of poorly sorted sediment, agitated and saturated with water, slide down slopes. Both solid and fluid forces strongly influence the motion, distinguishing debris flows from related phenomena such as rock avalanches, turbidity currents, and sediment-laden water floods. Whereas solid-grain interactions dominate momentum transfer in avalanches, and fluid turbulence dominates momentum transfer in turbidity currents and floods, solids and fluids must transfer momentum synergistically to sustain the type of motion that characterizes debris flows. By this rationale, many events identified as debris slides, debris torrents, debris floods, mudflows, mudslides, mudspates, and lahars may be regarded as debris flows (cf Varnes 1978, Johnson 1984, Pierson & Costa 1987). The diverse nomenclature reflects the diverse origins, compositions, and appearances of debris flows from quiescently streaming sand-rich slurries to tumultuous surges of boulders and mud.

Although debris flows can originate by various means, as when pyroclastic flows entrain and melt snow and ice (e.g. Pierson et al 1990) or when abrupt floods of water undermine and incorporate ample sediment (e.g. O'Connor et al 1997), mobilization from landslides predominates (Johnson 1984). Contrasting styles of deformation help discriminate mobilized debris flows from landslides that do not mobilize. Debris flows exhibit pervasive, fluid-like deformation that facilitates motion of even boulder-rich debris through tortuous channels, across gentle slopes, and around obstructions (Figure 1). Landslide motion is more rigid, with deformation localized along persistent slip surfaces or shear zones. The distinction between landsliding and debris flow is gradational and analogous to that between sand that slips incrementally along discrete failure surfaces, as may happen underfoot on a beach, and sand that flows rapidly, as may happen on a steep dune face (cf Jaeger & Nagel 1992, Jaeger et al 1996). However, effects of pore water give debris flows mobility that surpasses even that of dry, flowing sand (Iverson 1997). The qualitative difference between sliding and flowing motion, and the key role played by water and agitation in facilitating flow, have long been apparent to astute observers:

When a gentle slope of grit and shingle has been soaked like a sponge by rain or melting snows there may come a time when it slides off, . . . slipping into channels and gullies this mass . . . attains a higher speed and carries away soft material as well as rocks which it finds on its way. It is during this descent that the mudspate generally acquires its characteristic composition, for only by movement can an even mixture of liquid and solids be maintained.  
—W. R. Rickmers, *The Duab of Turkestan*. Cambridge University Press, 1913.

Landslides may completely or partially mobilize to form debris flows, and particular conditions must exist for mobilization to occur. Understanding these conditions has practical as well as scientific importance, for hazards and sediment transport associated with debris flows exceed those of comparably sized



*Figure 1* The west Dodson debris flows of February 8, 1996, entered this house situated on a fan at the mouth of a canyon about 60 km east of Portland, Oregon, and carried away owners' possessions without knocking the house from its foundation. This exemplifies the mobility of deforming debris-flow mixtures.

landslides that do not mobilize. Small debris flows occur commonly where hillsides or embankments that slope nearly at the angle of repose become saturated with water and fail (e.g. Kesseli 1943, Rodine 1974). Great debris flows may result from numerous, small slope failures that subsequently coalesce (e.g. Fairchild 1987, Rodolfo et al 1996) (Figure 2), from flow enlargement due to incorporation of bed and bank debris (e.g. Pierson et al 1990, Bovis & Dagg 1992), or from large, individual landslides that mobilize partially or almost totally (e.g. Plafker & Ericksen 1978, Vallance & Scott 1996) (Figure 3). Mobility may be enhanced by entrainment of water along the way (Pierson & Scott 1985). In all these cases, however, gravitational failure of discrete volumes of water-laden sediment or rock initiates the process.

In this review we examine findings from diverse disciplines in an attempt to synthesize a coherent, quantitative description of the mechanisms by which landslides mobilize to form debris flows. As a vehicle for synthesis, we adopt a perspective of debris flows that emphasizes results of controlled experiments and principles of modern soil mechanics, grain-flow mechanics, and mixture mechanics (Iverson 1997). Other overviews adopt perspectives that highlight Bingham or Bagnold models of debris flows (e.g. Johnson 1984, Takahashi 1991) or the hydrologic and geologic factors that influence mobilization in

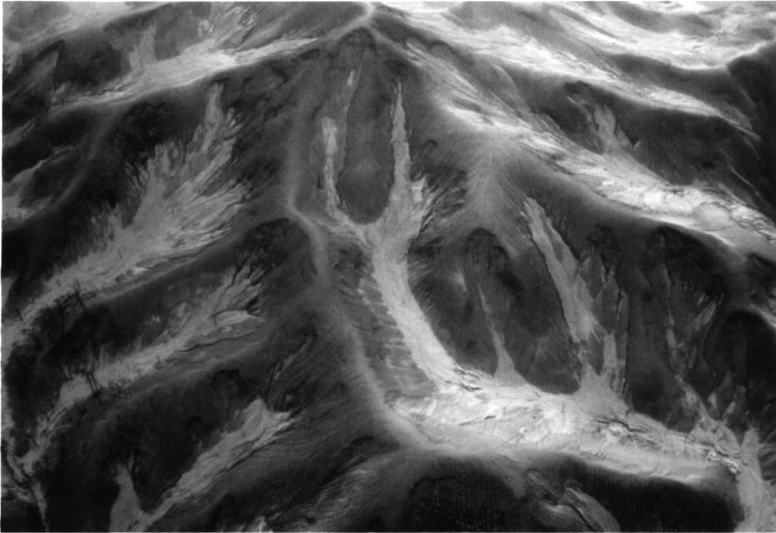


*Figure 2* Oblique aerial photographs of distributed source areas from which small debris flows issued and coalesced to form large flows. *Top photo*: roughly 10 km southwest of Mount Pinatubo, Phillipines, June 1991. Topographic relief is about 50 m. Removal of a mantle of freshly deposited pumice by debris flows highlights source areas and flow paths. (Photo courtesy of J. Major.) *Bottom photo*: about 10 km northeast of Mount St. Helens, Washington, February 1996. Topographic relief is about 600 m. Removal of snow cover by debris flows highlights source areas and flow paths.

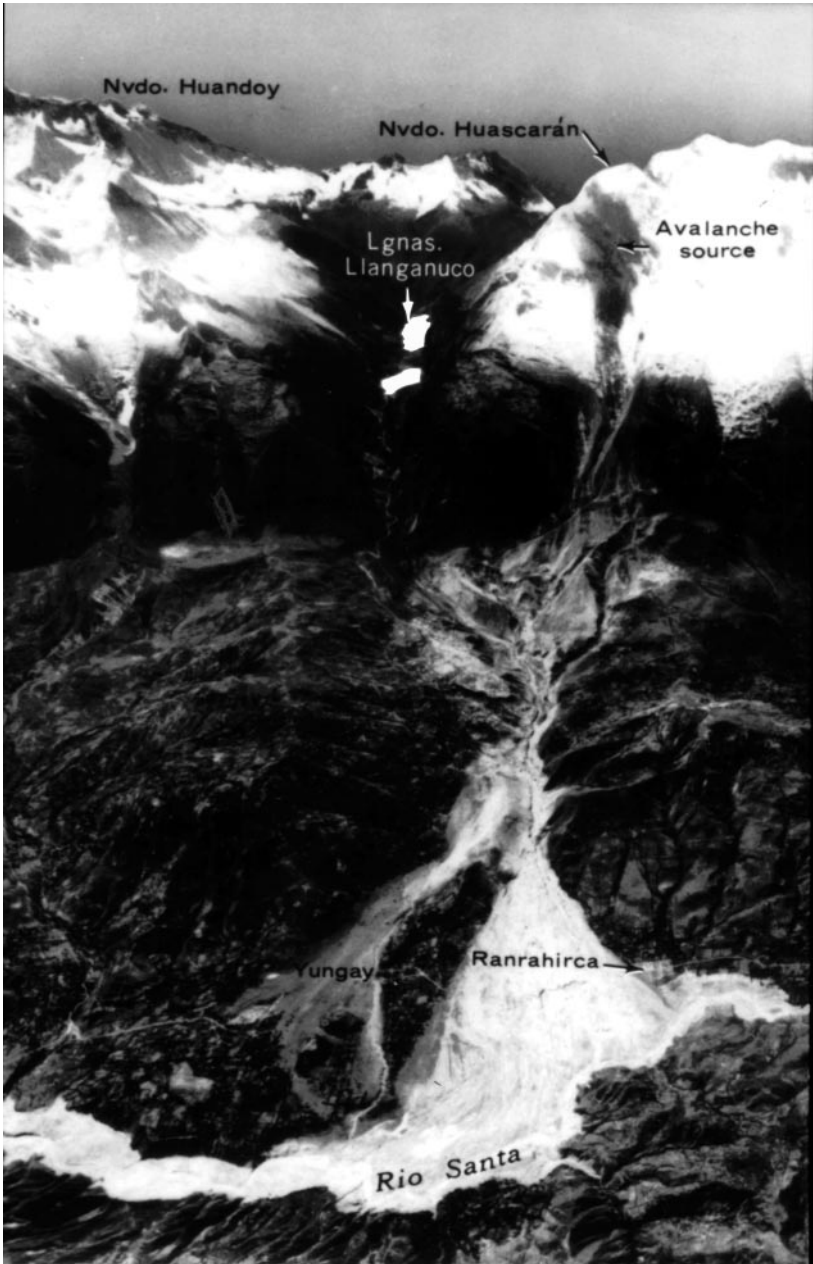


*Figure 3* Source area and upper runout path of a large debris avalanche that partially mobilized to form a debris flow, Nevados Huascarán, Peru, 1970. Topographic relief is about 4100 m. The  $\sim 10^8\text{-m}^3$  avalanche-debris flow destroyed the city of Yungay and part of the city of Ranrahirca, and continued down the Rio Santa more than 100 km to the sea. (Photo courtesy of G. Plafker.)

specific settings (e.g. Campbell 1975). Where appropriate, we compare and contrast these previous perspectives with the present one.

## BASIC CONCEPTS: COULOMB FAILURE, EFFECTIVE STRESS, PORE PRESSURE, LIQUEFACTION, CRITICAL STATE, AND GRANULAR TEMPERATURE

Principles of soil mechanics (e.g. Schofield & Wroth 1968, Lambe & Whitman 1979), grain-flow mechanics (e.g. Savage 1984, Campbell 1990), and mixture mechanics (e.g. Atkin & Craine 1976) provide a framework for assessing debris-flow mobilization. One principle involves the Coulomb failure rule, which describes the criterion for slip along discrete surfaces in granular materials of many types. Data accumulated since Coulomb's (1773) enunciation of this rule show that shear failure in masses of unlithified regolith and pervasively fractured rock (lumped under the term *soil* hereafter) occurs if stresses grossly obey the equation

$$\tau = \sigma' \tan \phi + c, \quad (1)$$

in which  $\tau$  is the mean shear stress acting on the failure surface,  $\sigma'$  is the mean effective normal stress (positive in compression) acting on the failure surface,  $\phi$  is the angle of internal friction of the soil, and  $c$  is the cohesive (nonfrictional) component of the soil strength. Theory and measurements of slowly deforming Coulomb materials show that shear stresses never exceed those described by Equation 1 (e.g. Mandl & Fernandez-Luque 1970, Adams & Briscoe 1994). Instead, stresses in failing Coulomb materials adjust so that they satisfy this equation wherever failure occurs. The angle  $\phi$  reflects both the intrinsic surface friction of individual soil clasts and the degree to which clasts interlock geometrically, which may change somewhat as failure proceeds. The product  $\sigma' \tan \phi$  determines the frictional component of the soil strength. The cohesion  $c$  depends chiefly on electrostatic forces between clay particles and on cementation due to secondary mineralization between soil clasts (Mitchell 1976). Cohesion commonly contributes little strength, but this contribution can exceed the frictional strength where effective stresses are especially low—at shallow depths on steep slopes, for example. Soil on slopes may also possess apparent cohesion due to the strength of interpenetrating roots of plants (e.g. Greenway 1987). Cohesion tends to be destroyed, however, if large soil displacements occur (Skempton 1985).

The Coulomb failure rule (Equation 1) includes the effective normal stress,  $\sigma'$ , which accounts implicitly for the effects of pore-fluid pressure,  $p$ . Unlike the grain-contact stresses,  $\sigma'$  and  $\tau$ , the fluid pressure in static soil is isotropic, and fluid shear is assumed to dissipate no energy (Bear 1972). The effective

normal stress is conventionally defined by

$$\sigma' = \sigma - p, \quad (2)$$

where  $\sigma$  is the total normal stress that would be measured, for example, on a flat plate positioned flush with the prospective failure surface. This expression for  $\sigma'$  dates at least to Terzaghi (1936), but was probably conceived in much earlier work (de Boer & Ehlers 1990). More sophisticated definitions of effective stress are also possible (e.g. Passman & McTigue 1986), but none has superseded Equation 2 as a useful description of the stresses that cause Coulomb failure.

The combination of Equations 1 and 2 can give an unrealistically simple impression of the factors that govern slope failure, because the equations do not account for the stress and pore-pressure fields that determine  $\tau$ ,  $\sigma'$ , and  $p$  on a slip surface. For example, one might infer from these equations that increased pore pressures necessarily increase the potential for Coulomb slope failure. This assumption is erroneous, as demonstrated by slopes submerged under great depths of static water, where pore pressures are great but  $\sigma$  is comparably great owing to fluid pressure acting on the boundary of the submerged sediment. The spatial distribution of pore pressures [ $p(x,y,z)$  where  $x$ ,  $y$ , and  $z$  are space coordinates] in addition to the magnitude of pore pressure on a prospective slip surface, determines the Coulomb failure potential. The spatial distribution of solid grain stress is similarly important (cf Iverson & Reid 1992).

The pore-pressure distribution  $p(x,y,z)$  is related in a simple way to the distribution of hydraulic head  $h(x,y,z)$ , which drives groundwater flow (e.g. Bear 1972):

$$p = \gamma_w(h + z). \quad (3)$$

Here  $z$  is a space coordinate oriented vertically downward, in the direction of gravitational acceleration, and  $\gamma_w$  is the unit weight of the pore water. The origin for  $z$  may be defined arbitrarily, but in the present context it is convenient to assume  $z = 0$  at a point on the ground surface. Groundwater flux is represented by the Darcian specific discharge,  $\vec{q}$  (Bear 1972):

$$\vec{q} = K \cdot \nabla h, \quad (4)$$

where  $K$  is the (tensor-valued) hydraulic conductivity of the soil. From Equations 1–4 it is clear that assessment of Coulomb slope failure requires knowledge of the groundwater-flow field, which is tantamount to knowledge of the pore-pressure distribution.

The pore-pressure (or head) distribution also determines the potential for soil liquefaction. The term liquefaction is used here in a relatively restrictive sense to describe a condition in which the ambient pore pressures produce a state of zero effective stress in a soil mass (cf Youd 1973, Casagrande 1976). This

liquefied state is equivalent to a so-called quick state, and it may be achieved as a result of either static or transient stressing. With a geostatic stress field, the condition for liquefaction requires that the vertical pore-pressure gradient equals the vertical gradient of the total normal stress,  $\sigma$ , which equals the unit weight,  $\gamma_t$ , of the superincumbent, water-laden soil:

$$\frac{\partial p}{\partial z} = \frac{\partial \sigma}{\partial z} = \gamma_t. \quad (5)$$

Together with Equation 2, Equation 5 implies that  $\sigma' = 0$  everywhere in the soil mass and that the frictional strength of the soil is zero. If strength due to cohesion is also zero, soil in which Equation 5 is satisfied can flow quite readily—like a liquid. Soil with nonzero cohesion can liquefy in this manner only if the cohesive bonds are broken. During an earthquake or landslide, for example, transient stressing may disrupt soil structure and cohesive bonds, elevate pore pressures, and partially or completely liquefy the soil (Holzer et al 1989, Iverson & LaHusen 1989, Eckersley 1990). Understanding how such a liquefied state may occur in landslides, and understanding how transient liquefaction can produce feedbacks that enhance soil deformation, is critical to understanding debris-flow mobilization.

If soil begins to shear as a result of either Coulomb failure or liquefaction, grains in the shearing zone must rearrange their positions. If the shear rate is sufficiently small that rearranging grains maintain virtually continuous contact with one another, the shearing may be regarded as quasistatic, and the soil develops a steady, critical-state bulk density (Schofield & Wroth 1968, Atkinson 1981). In principle, the same critical-state bulk density is attained regardless of the density prior to shearing. Densely packed soils dilate to reach the critical state, and loosely packed soils contract (Figure 4). Contraction can elevate pore-fluid pressures if the rate of pore-space reduction surpasses the rate at which induced fluid pressures can dissipate. Pore pressures elevated in this manner can produce classical liquefaction as described by Equation 5, and this type of liquefaction or near-liquefaction has been suggested as a mechanism for debris-flow mobilization (Sassa 1984, Ellen & Fleming 1987).

A phenomenon known as granular temperature becomes important when soil deformation rates exceed quasistatic limits. Granular temperature measures the degree of agitation of solid grains, which influences the mixture bulk density and the ability of grains to avoid interlocking and move past one another. Granular temperature,  $T$ , is determined by the ensemble average of grains' velocity fluctuations,  $v'$ , about their mean velocities (Campbell 1990):

$$T = \langle v'^2 \rangle = \langle (\vec{v} - v_x)^2 \rangle, \quad (6)$$

where  $\vec{v}$  is the instantaneous velocity of a solid grain,  $v_x$  is its average (down-slope) velocity, and  $\langle \rangle$  denotes the ensemble average of all grains. Defined in

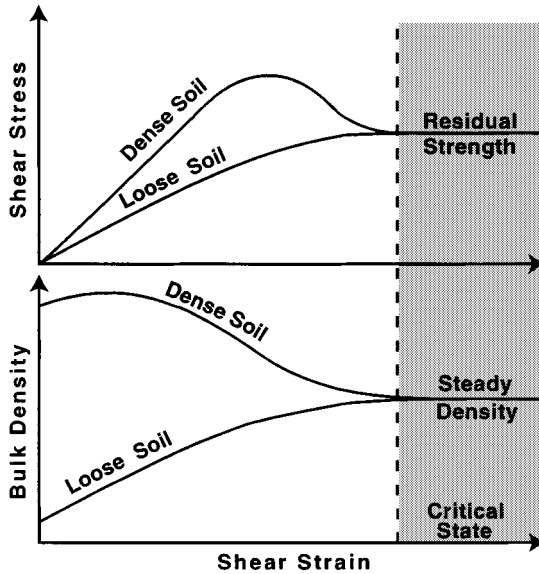


Figure 4 Qualitative changes in shear stress and strength and bulk density of dense and loose soils during the initial stages of quasistatic shear deformation.

this manner,  $T$  may be interpreted as twice the fluctuation kinetic energy per unit mass of grains.

Granular temperature derives its name from the analogy between grain fluctuation kinetic energy and the molecular kinetic energy that determines the thermodynamic temperature of a gas. Just as higher temperatures reduce the density and enhance the fluidity of an ideal gas, higher granular temperatures reduce the concentration of solids and enhance the fluidity of debris flows (Iverson 1997). Unlike gas temperature, however, granular temperature cannot be maintained in the absence of energy exchange with the environment, because grain-velocity fluctuations cause energy dissipation due to grain interactions and pore-fluid flow. Granular temperature can be generated and maintained only by continual conversion of bulk translational energy to grain fluctuation energy. In debris flows, bulk translational energy is supplied by downslope travel of the moving mass, and conversion of bulk translational energy to grain fluctuation energy occurs as grains shear along irregular surfaces (Figure 5) (Iverson 1997). If granular temperature generated along a landslide slip surface is transferred sufficiently into adjacent soil, the localized slip can cause more widespread slip, which can mobilize the landslide into a flow.

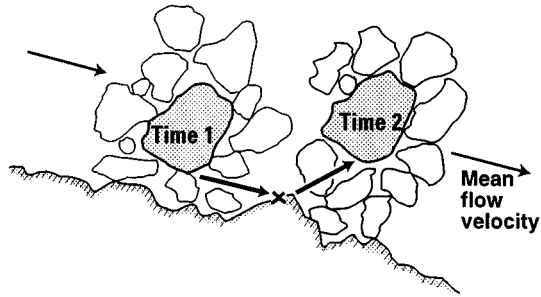


Figure 5 Schematic depiction of granular temperature generation by conversion of downslope translational energy to slope-normal fluctuation energy via grain collision with a rough bed.

The mechanics of granular temperature generation differ in subtle but important ways from those of acoustic fluidization or dispersive stress. Acoustic fluidization (Melosh 1979, 1987) occurs if propagating elastic waves briefly but repeatedly reduce grain-contact stresses such that the Coulomb rule (Equation 1) is satisfied pervasively, which permits a granular mixture to flow. Production of granular temperature is a more general, kinematic phenomenon that need not depend on elastic waves. Granular temperature spreads from point to point by a conduction rather than wave-propagation process (cf Campbell 1990). Granular temperature arises from more-or-less random grain interactions that can dilate and disperse a granular mixture—as envisaged by Bagnold (1954) in his dispersive-stress model—but granular temperature extends Bagnold's (1954) ideas about grain interactions beyond the limits of the gravity-free environment and homogeneous shear field considered in his experiments and analysis. Transformation from localized landslide slip to widespread flow that occurs during debris-flow mobilization involves both gravity-driven inhomogeneous shear deformation and concomitant conduction of granular temperature (Iverson 1997). Bagnold's (1954) concept of dispersive stress is too restrictive to assess these phenomena.

Effects of granular temperature on steady flows of dry granular materials have been demonstrated by detailed analyses using kinetic theory (e.g. Jenkins & Savage 1983, Lun et al 1984), by numerical simulations (Campbell 1990, Walton 1993), and by laboratory experiments (Drake 1990, 1991). Numerical simulations have also clarified how granular temperature affects the transition from quasistatic, localized slip to widespread, agitated flow (Zhang & Campbell 1992). However, with a few exceptions (Iverson & LaHusen 1989, McTigue & Jenkins 1992, Pak et al 1995), little work has emphasized the simultaneous effects of granular temperature and pore-fluid pressure.

In this review we consider how debris flows can be mobilized by three processes, which perhaps operate simultaneously and synergistically: (a) widespread

Coulomb failure within a soil mass, (b) liquefaction of a soil mass by high pore-fluid pressures, and (c) production of granular temperature in a soil mass that becomes agitated as it moves downslope. In some instances the influence of one or two of these processes may dominate. However, at least partial liquefaction by high pore pressures appears to influence all debris flows, for this is the phenomenon that distinguishes debris flows from flows of drier sediment (Iverson 1997). Liquefaction can temporarily impart debris flows with near-zero rigidity, so that massive debris flows may sweep paradoxically around and through structures without displacing them from their foundations (Figure 1).

## MOBILIZATION HYPOTHESES

Several hypotheses have been advanced to explain mobilization of debris flows. Although qualitative hypotheses have existed for more than half a century (e.g. Kesseli 1943), here we emphasize hypotheses that have been formalized, at least in part, in quantitative models. The models generally focus on failure and mobilization of an infinite slope of homogeneous, isotropic soil. An infinite slope is a convenient mathematical idealization used to specify an inclined, tabular soil mass with lateral dimensions much greater than its thickness, which is a suitable approximation for many sites of debris-flow mobilization (Figure 6). An infinite slope is mechanically one-dimensional: All pertinent quantities vary as functions of only a single space coordinate, which is directed normal to the slope surface. This renders the slope statically determinate, meaning that stresses can be calculated from statics alone, without any assumptions about soil rheology. Relatively unambiguous conclusions thus can be drawn about the stress field during Coulomb failure of infinite slopes and about the similarity of this stress field to that required for sliding deformation to transform to flow. Mobilization hypotheses also generally assume that the hillslope soil contains or acquires sufficient water to saturate virtually all pore spaces.

One hypothesis for mobilization derives from Johnson's (1965, 1970, 1984) Bingham model of debris-flow motion. The Bingham model assumes that soil can flow only if shear stresses exceed its yield strength, which is equivalent to the Coulomb strength defined by Equation 1 but is treated as an intrinsic material property unaffected by dynamic changes in soil friction, porosity, pore pressure, or granular temperature. Johnson and his associates (Johnson & Rahn 1970, Rodine 1974, Ellen & Fleming 1987) hypothesized that an infinite slope of hillslope soil with a particular water content must exceed a critical thickness to mobilize as a debris flow, for only then can shear stresses at the base of the soil exceed the Bingham yield strength (Figure 7). This requirement leads to a conceptual dilemma: If changes in hillslope stress and/or strength culminate in Coulomb slope failure, mechanics dictate that failure must occur at only the depth where the shear stress equals the Coulomb yield strength; yet to



*Figure 6* Source area and upper runout path typical for small debris flows, Kuliouou Valley, Oahu, Hawaii, January 1, 1988. The length (42 m) and width (16 m) of the source area greatly exceed the thickness (1–2 m) of the failed soil mass, indicating that a one-dimensional infinite-slope analysis might be appropriate. The average slope angle is  $32^\circ$ .

instigate Bingham flow, failure must propagate to greater depths, where shear stress exceeds the yield strength. This dilemma can be overcome by treating the yield strength or stress field not as fixed but rather as a function of variables such as soil porosities, pore pressures, and friction angles, which may change as failure occurs. Most advocates of the Bingham model, such as Johnson & Rahn (1970), Rodine (1974), and Ellen & Fleming (1987), have recognized the need to generalize the model in this way. However, such a generalization can be accomplished rigorously only by replacing the one-phase Bingham model with a formulation that explicitly represents the distinct effects of debris flows' solid and fluid constituents (Iverson 1997).

Takahashi (1978, 1981) presented an alternative hypothesis for mobilization, which is compatible with his model of debris flows as a water-saturated inertial grain flows governed by Bagnold's (1954) concept of dispersive stress (Takahashi 1980). Others have proposed similar hypotheses (e.g. Vallejo 1979). Because the relation between grain shear and normal stresses in Bagnold's dispersive-stress model is functionally identical to that in the quasistatic Coulomb rule (Equation 1) with  $c = 0$  (cf Savage 1984), Takahashi's mobilization

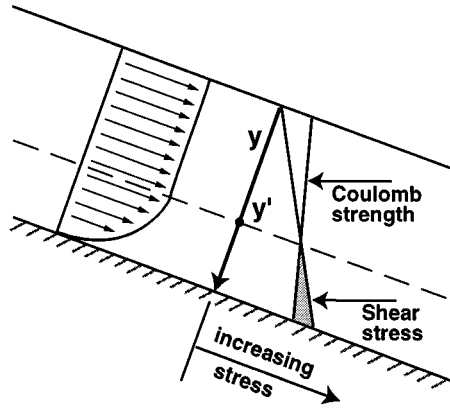


Figure 7 Schematic profile illustrating mobilization of a Bingham flow on an infinite slope. Below depth  $y = y'$ , shear stress must exceed the yield strength (*shaded region*), which is difficult to reconcile with the mechanics of Coulomb slope failure.

model is essentially a Coulomb failure model. Indeed, his mobilization model emulates the well-known Skempton-DeLory (1957) model for Coulomb failure of infinite slopes with slope-parallel seepage—for the special case where  $c = 0$  and the slope is fully saturated. The model neglects the possibility of alternative pore-pressure distributions and the potential for soil liquefaction. Hypothetically, a debris flow might mobilize by widespread Coulomb failure of a cohesionless, saturated slope that does not liquefy, but the requirement of slope-parallel groundwater flow mandates that this can occur at only one slope angle,  $\theta$ , for a soil with a particular  $\phi$  and  $\gamma_i$  (Iverson & Major 1986). Takahashi (1978, 1981) circumvented this restriction by assuming that water not only saturates the slope but also flows across the slope surface (Figure 8). The surcharge imposed by an arbitrary thickness of surface water causes the driving stress to exceed the Coulomb resistance throughout an arbitrary soil thickness, thereby triggering widespread failure and flow in slopes of varying steepness. However, this scenario presents a mechanical difficulty that parallels that of the Bingham model: Why doesn't failure occur at the shallowest possible depth as shear stress in the soil increases in response to increasing surface-water depths? Together with the assumption of slope-parallel groundwater flow, the assumption of a surface-water surcharge also restricts the angles of failing slopes to less than  $\phi/2$ , approximately (cf Lambe & Whitman 1979, Iverson 1992). This angle corresponds to less than  $25^\circ$  for most soils (which have  $\phi < 50^\circ$ ), whereas hill-slope angles in the  $25\text{--}45^\circ$  range are observed most commonly at sites where debris flows mobilize from landslides (Table 1). Consequently, Takahashi's model might best apply where debris flows mobilize from flash floods that abruptly

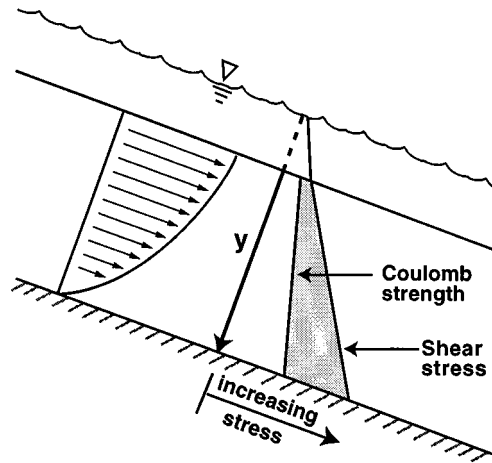


Figure 8 Schematic profile illustrating mobilization of an inertial grain flow on an infinite slope, as in the Takahashi model. The shear stress must exceed the Coulomb strength through at least part of the soil thickness (*shaded region*). Takahashi (1991, p. 64) presents variations of this basic mechanism, but in all cases the surcharge of water above the ground surface at  $y = 0$  is essential.

impose surface-water surcharges in relatively gently sloping, sediment-choked channels (Takahashi 1991). Nonetheless, when applied to channels, his model of mobilization disregards the possible role of liquefaction, just as it does when applied to slopes.

Other hypotheses for debris-flow mobilization emphasize the principles of soil mechanics (e.g. Anderson & Sitar 1995). These hypotheses generally assume that debris flows mobilize as a result of at least partial liquefaction caused by pore-pressure growth beyond hydrostatic values, rather than by shear-stress growth beyond a fixed yield value. Consequently, soil mechanics hypotheses rely fundamentally on the concept that debris flows consist of two-phase solid-fluid mixtures, in which solid and fluid stresses need not balance (Iverson 1997). Soil mechanics hypotheses differ, however, in explaining how pore-fluid pressures exceed hydrostatic levels. The simplest hypothesis supposes that pore pressures resulting from the ambient groundwater flow field practically suffice to liquefy the soil once Coulomb failure occurs and cohesive soil bonds are disrupted (Iverson & Major 1986, Denlinger & Iverson 1990). This requires groundwater flow with a component directed vertically upward. Alternatively, many investigators have hypothesized that debris-flow mobilization occurs only in loose soils that have in situ bulk densities less than the critical-state density (e.g. Casagrande 1976); contraction of these loose soils during quasistatic failure can drive pore pressures upward as the soil approaches the

**Table 1** Slope angles measured at sites of debris-flow initiation from landslides in localities where numerous debris flows resulted from one or more hydrologic events

Reference	Location	Slope angles (degrees)
Temple & Rapp 1972	Tanzania	28–44
O'Loughlin 1972	Southwestern British Columbia, Canada	24–48
Lumb 1975	Hong Kong	25–45
Campbell 1975	Southern California, USA	27–56
Selby 1976	New Zealand	32–34
Statham 1976	Wales	27–37
Pomeroy 1980	Pennsylvania, USA	20–40
Heller 1981	Northwestern Washington, USA	20–40
Ellen et al 1988	Northern California, USA	20–50
Pierson et al 1992	Hawaii, USA	30–60
Rickenmann & Zimmermann 1993	Switzerland	27–39

critical state (Sassa 1984, Ellen & Fleming 1987, Kramer 1988). Geotechnical engineers conventionally deem this type of soil behavior as undrained, because it mimics behavior observed in undrained laboratory test cells. Soils on natural hillslopes cannot be truly undrained, however, because they do not reside in sealed containers. The crucial issue entails the time scale of drainage (pore-pressure dissipation) vs that of soil contraction (cf Iverson & LaHusen 1989). If porosity declines during failure more rapidly than pore pressures can equilibrate, attendant growth of pore pressures can potentially liquefy and mobilize the soil (cf Hutchinson 1986, Eckersley 1990, Sasitharan et al 1993).

Some debris flows originate in dense soils that dilate as they fail (Fleming et al 1989, Anderson & Sitar 1995), and this observation has motivated additional soil-mechanics-based hypotheses to explain production of excess pore pressures. Most of these hypotheses emphasize that the dynamics of the failure process modifies stresses from their pre-failure quasistatic values. For example, dynamic pore-pressure fluctuations that accompany shearing on discrete failure surfaces can propagate diffusively from their source and change the effective-stress distribution to enhance the potential for liquefaction (Iverson & LaHusen 1989, Iverson 1993, Kytomaa 1993). Perturbations in solid-gain stresses due to the failure process itself or extraneous vibrations may have the same effect (Anderson & Sitar 1995). Indeed, growth of fluctuations in both solid stress and fluid stress associated with growing granular temperature (McTigue & Jenkins 1992) may allow dense soils to mobilize. The role of such fluctuations can be particularly important where debris flows mobilize from rather dense masses of fractured rock that gain much granular temperature by tumbling down steep slopes (e.g. Plafker & Ericksen 1978).

Another soil-mechanics-based hypothesis for debris-flow mobilization derives from novel laboratory soil tests by Vaid & Thomas (1995), who observed that even dense soils can contract during failure under extensional states of stress. Since most landslides develop tension cracks and elongate conspicuously as they fail, extensional stresses most likely are induced (Savage & Smith 1986, Baum & Fleming 1991). Increased pore pressures might therefore arise as contraction occurs in failing, dense soils. More data are needed to substantiate this hypothesis.

## HYDROLOGIC TRIGGERS

Shallow groundwater flow in response to rainfall, surface runoff, and snowmelt triggers most subaerial debris flows. Rainfall triggering of debris flows and other landslides in steep terrain has been the object of intensive study. Investigations have included assessments of empirical relationships between debris-flow occurrence and rainfall intensities and durations (e.g. Caine 1980, Cannon & Ellen 1985), deterministic assessments of the hydrologic processes involved (e.g. Campbell 1975, Humphrey 1982, Leach & Herbert 1982, Reid et al 1988, Buchanon et al 1990, Johnson & Sitar 1990, Wilson & Wieczorek 1995), and deterministic analyses that account explicitly for uncertainty in soil hydraulic parameters such as  $K$  and  $h$  (Reddi & Wu 1991). Quantitative synthesis of these investigations and other pertinent studies of hillslope hydrology (e.g. Kirkby 1978, Zaslavsky & Sinai 1981) is beyond the scope of this review. Instead we summarize briefly the qualitative elements of hillslope hydrology that can most strongly influence the mechanics of debris-flow mobilization.

The key hydrologic requisites for debris-flow mobilization are sufficient water to saturate (or nearly saturate) the soil and sufficient pore-water pressure and/or weight to initiate Coulomb slope failure. If, in addition, the pore-water pressure at the time of slope failure is close to that required to liquefy the soil, the potential for flow mobilization is enhanced (Iverson & Major 1986). The weight of added water plays a mechanical role independent of pore pressure only if cohesion contributes significantly to the Coulomb soil strength (as demonstrated by Equations 7a–d in the next section). Although shallow slope failures may be triggered under wholly unsaturated conditions by infiltration that increases the soil weight or reduces the ambient soil moisture suction (Brand 1981), most studies indicate that debris flows result from development of positive pore pressures that accompany saturation.

Positive pore pressures in hillslope soil that might mobilize to form a debris flow can develop by two means; direct infiltration of water at the slope surface, and groundwater inflow from the adjacent soil or rock. Infiltration generally involves unsaturated flow in a dominantly vertical direction, although lateral

unsaturated flow may redistribute the moisture (e.g. Weyman 1973, Harr 1977, Phillip 1991). Saturation and positive pore pressures commonly develop when infiltrating water encounters soil with lower permeability, and transient water-table perching occurs (Campbell 1975, Reid et al 1988). Alternatively, infiltrating water may elevate the regional water table until it intersects near-surface soils. Significant lateral inflow to these soils may occur by saturated groundwater flow from adjacent materials. A sloping water table, three-dimensional topographic convergence, and other factors may help direct the saturated flow laterally (Anderson & Burt 1978).

Traditional groundwater-flow models generally treat soils and rocks as continuous porous media that obey Darcy's law, but field evidence indicates that the hydrology of some natural slopes is strongly influenced by discontinuities such as fractures and macropores. Sidle & Swanston (1982), Pierson (1983), and McDonnell (1990), for example, reported the potentially dominating influence of macropores such as root channels and animal burrows on hillslope hydrology and slope stability. Other investigators (e.g. Wilson & Dietrich 1987, Mathewson et al 1990, Montgomery et al 1990) have studied field sites in which bedrock fractures or blockages help channel groundwater into overlying soils. Concentrated water discharge into overlying soil resulting from either subsurface channels or blockages is accompanied by locally elevated pore pressures and outward-directed hydraulic gradients that enhance the potential for slope failure and liquefaction (Rogers & Selby 1980, Reid & Iverson 1992). Sophisticated numerical models that treat the coupling between flow in fractures and variably saturated flow in adjacent soil have been developed (e.g. Abdel-Salam & Chrysiopolous 1996), but to our knowledge they have not been applied to sites of debris-flow mobilization.

Perhaps the most important hydrologic distinction between slopes that merely fail and those that mobilize to form debris flows is the high water content required for mobilization. Limited field data suggest that soils that mobilized to form debris flows were saturated or nearly saturated prior to failure (Sidle & Swanston 1982, Reid et al 1988, Johnson & Sitar 1990). However, attainment of high (nearly saturated) water contents in steep subaerial slopes presents a mechanical difficulty. A cohesionless subaerial slope standing at the angle of repose can sustain no positive pore pressure without failing. Yet sites where subaerial debris flows originate commonly have slopes in the 30–40° range (Table 1), which typifies angles of repose of granular soils. A critical question, then, concerns how high water contents are attained without pore pressures causing preemptive failure of the slope—or, alternatively, how the slope remains stable long enough to become nearly saturated.

Infiltration and unsaturated water flow is a complex and nonlinear process (e.g. Bear 1972, Phillip 1991); nevertheless, simple inferences from Equation 3

show that a slope can become fully saturated yet possess zero pore pressure if steady infiltration occurs under the condition  $\partial h/\partial z = -1$ . If  $\partial h/\partial z > -1$ , positive pore pressures exist, whereas  $\partial h/\partial z < -1$  indicates the existence of negative pore pressures (suction). Combined with Darcy's law (Equation 4), the condition  $\partial h/\partial z = -1$  implies that the downward flux of groundwater,  $q_z$ , equals the saturated hydraulic conductivity,  $K$ , of the soil. With prolonged rainfall at intensities greater than or equal to  $K$ , a saturated zone will develop at the soil surface and propagate downward. However, water within this saturated zone attains little or no positive pore pressure. Moreover, after rainfall ceases, the soil can for a time remain tension-saturated even as gravity drainage occurs and negative pore pressures develop. A subsequent burst of high-intensity rainfall can cause the tension-saturated zone to develop positive pore pressures almost instantaneously, provided there is a water table or stratum of low permeability beneath it. Such a rapid response mechanism was observed by Gillham (1984) in a capillary fringe above a water table. A mechanism of this type may have initiated two miniature debris flows in hillslope sprinkling experiments conducted by Iverson (1980), but few, if any, data are available to demonstrate its widespread importance.

A better documented scenario involves gradual growth of positive pore pressures within the saturated zone beneath a rising water table. If rainfall infiltration occurs at rates smaller than  $K$ , then  $\partial h/\partial z < -1$  and moisture contents of wetting soil above the water table may remain well below saturated levels. The water table may be regional or perched locally above a zone of low permeability and may be overlaid by a capillary fringe. In any case the saturated zone in the soil grows from the bottom up rather than from the top down. Bottom-up growth of the saturated zone at a site of potential slope failure can also result from influx of water from adjacent soil or rock. Regardless of the details, under any of these conditions a steep slope of cohesionless soil will fail before the slope is saturated (see Equations 7a–d in the next section), which poses a difficulty for debris-flow mobilization.

At least two phenomena might alter this basic picture and allow debris flows to mobilize from slopes that become saturated from a rising water table: (a) The simplest possibility is that cohesion inhibits failure until the slope becomes saturated and significant positive pore pressures develop. In such circumstances the slope can even develop hydraulic head gradients with an upward vertical component that enhances the potential for liquefaction. As quantified in the next section, relatively modest cohesions of a few kilopascals can make this process viable. (b) Another possibility is that soil-water contents in a significant fraction of the soil remain less than saturated at the time of slope failure. When positive pore pressures at depth trigger failure, water contents in the unsaturated zone rise to saturated or near-saturated levels as a consequence of soil contraction

that originates at slip surfaces but spreads to adjacent soil by conduction of granular temperature. Volumetric contraction during failure appears unlikely to reduce pore space by more than about 20%, however. Saturation due to contraction consequently requires preceding rainfall at rates close to  $K$ , soil-water retention characteristics that permit a state of tension-saturation or near-saturation to persist during gravity drainage, or a rising capillary fringe above a rising water table. Taken together, these two phenomena provide a reasonable explanation for saturation of most steep slopes that produce debris flows. However, almost no field data have sufficient detail to lead to firm conclusions about hydrologic conditions in landslides that have spawned debris flows. Theory and experiments described in subsequent sections fill some of the voids in our understanding.

## ELEMENTARY MECHANICS: INFINITE SLOPES

Before examining more complicated facets of debris-flow mobilization, we quantify the mechanics of Coulomb failure and subsequent sliding in an infinite slope inclined at a uniform angle  $\theta$  (Figure 9). This quantification helps codify the relationships between the alternative hypotheses for mobilization described above and also helps synthesize a unifying hypothesis. We develop a unified mechanical model by removing Takahashi's assumption of slope-parallel groundwater flow, assessing the relationship between Coulomb failure and liquefaction, and considering the role of granular temperature and soil volume change in an infinite-slope formulation.

### *Statics of Slope Failure and Liquefaction*

Conditions for Coulomb failure at any depth  $Y$  in an infinite slope inclined at the angle  $\theta$  can be represented by a factor-of-safety equation. A useful form of the equation imposes no arbitrary constraints on the ambient groundwater-flow (or pore-pressure) field, and it expresses the factor of safety,  $FS$ , as the sum of three dimensionless ratios (Iverson 1992):

$$FS = T_f + T_w + T_c, \quad (7a)$$

in which

$$T_f = \frac{\tan \phi}{\tan \theta} \quad (7b)$$

describes the ratio of frictional resisting strength to gravitational driving stress,

$$T_w = \frac{\left[ \frac{d}{Y} - 1 \right] \frac{\partial p}{\partial y} \tan \phi}{\gamma_t \sin \theta} \quad (7c)$$

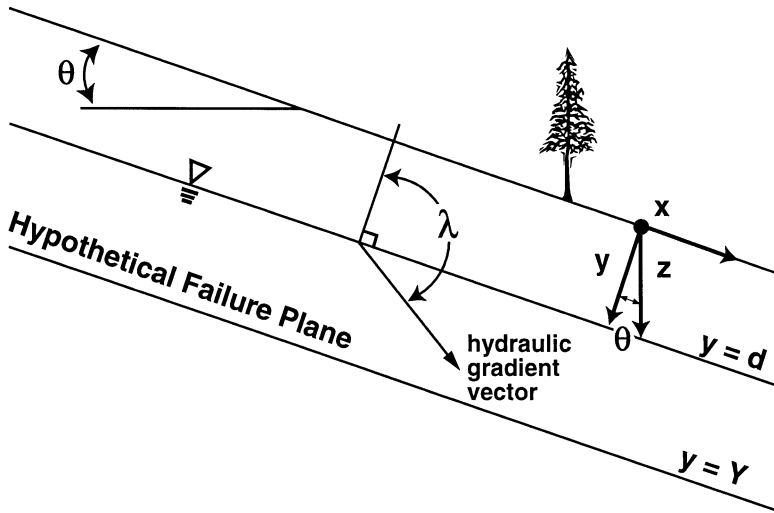


Figure 9 Schematic profile and definition of geometric parameters for an infinite slope with groundwater head gradient in an arbitrary direction  $\lambda$ . The angle  $\lambda$  is related to the head gradient magnitude,  $i$ , by  $\lambda = \sin^{-1}(\sin \theta / i)$  (modified from Iverson 1992).

describes the ratio of strength modification by groundwater to the gravitational driving stress, and

$$T_c = \frac{c}{\gamma_t Y \sin \theta} \tag{7d}$$

describes the ratio of cohesive strength to gravitational driving stress. In Equation 7c,  $d$  is the depth of the water table, where  $p = 0$ . The water table necessarily parallels the ground surface, as do all surfaces with constant  $p$  in infinite slopes (Iverson 1990). In Equations 7c and 7d,  $\gamma_t$  represents the depth-averaged total unit weight of saturated and unsaturated soil below and above the water table (cf Iverson 1992). If  $FS > 1$  in Equation 7a, resisting forces exceed driving forces, and the slope remains stable. Slope failure commences if  $FS = 1$ .

Some simple relationships apparent in Equations 7a–d help illuminate the factors that influence debris-flow mobilization. For example, Equation 7b does not contain the failure depth  $Y$ . Thus infinite slopes will fail simultaneously at all depths if pore pressures, cohesion, or variations in  $\phi$  that cause strength heterogeneity are absent. This pervasive Coulomb failure constitutes a type of flow mobilization, but it can occur only if  $\theta = \phi$ . Therefore, landslides on steep slopes (where  $\theta \approx \phi$ ) may be predisposed to mobilize into debris

flows—a contention supported by field observations (Table 1). Water-saturated, cohesionless slopes inclined at lesser angles can have the same predisposition if the pore-pressure distribution suffices to trigger failure. This is evident from Equation 7c, which lacks dependence on  $Y$  if  $d = 0$ . Cohesion necessarily inhibits mobilization due to pervasive Coulomb failure; Equation 7d shows that  $c \neq 0$  implies that failure can occur only at a specific depth  $Y$ .

The groundwater term (Equation 7c) has the most widely ranging influence on  $FS$ , and its connotations for debris-flow mobilization are perhaps more elusive than those of Equations 7b and 7d. In Equation 7c,  $T_w$  is negative as long as  $d < Y$  (i.e. a water table is present) and  $\partial p/\partial y$  is positive; thus groundwater generally tends to reduce  $FS$  and enhance the potential for Coulomb slope failure. Figure 10 depicts graphs that show how normalized values of  $\partial p/\partial y$  and  $T_w/T_f$  vary as the slope angle,  $\theta$ , and direction of the hydraulic head gradient,  $\lambda$ , vary in saturated slopes (cf Iverson 1992). As the direction of the head gradient varies, the magnitude of  $\partial p/\partial y$  necessarily varies, which greatly influences the potential for Coulomb failure. Failure potential is most strongly enhanced if the head gradient has a component directed vertically upward ( $\lambda < 90^\circ - \theta$ ). Then  $\partial p/\partial y > \gamma_w \sec \theta$  and  $\partial p/\partial z > \gamma_w$ , indicating that the vertical pore-pressure gradient exceeds hydrostatic. Vertical pore-pressure gradients that exceed hydrostatic also enhance liquefaction potential, as represented in Equation 5.

Evaluation of the gradient of pore pressure (or groundwater head) necessary for liquefaction involves some ambiguity even for simple, infinite slopes. The ambiguity stems from the fact that principal stresses under sloping surfaces are not necessarily aligned in the slope-normal and slope-parallel directions, and the vertical normal stress is not necessarily geostatic ( $\sigma_{zz} \neq \gamma_t z$ ) (cf Lambe & Whitman 1979, p. 193; Vaughan & Kwan 1984; Kramer 1988). Which normal-stress component provides the resistance that is most critical for inhibiting liquefaction? Is a liquefaction criterion as simple as Equation 5 applicable?

Quantitative constraints on the applicable liquefaction criterion can be deduced for cohesionless infinite slopes in a state of Coulomb limiting equilibrium ( $FS = 1$ ). In such slopes the principal effective stresses are determined exactly. For the steeply inclined slopes that are most likely to generate debris flows (see Table 1), the assumption that in situ stress states mimic limit-equilibrium stress states is probably reasonable (Anderson & Sitar 1995). Of course, slopes at limiting equilibrium can be inclined at any angle  $\theta$ , provided that the groundwater term  $T_w$  suffices to provoke failure.

Figure 11 depicts the state of stress for some examples of cohesionless infinite slopes that satisfy Coulomb limiting equilibrium. Pictorial representations of the principal effective stresses and the corresponding Mohr's circle representations are shown. Coulomb failure envelopes form tangents to the Mohr's

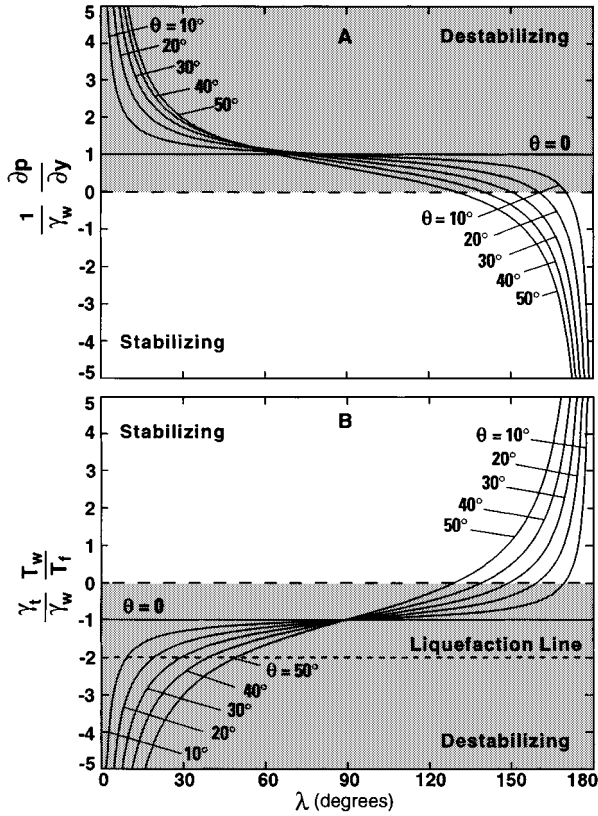


Figure 10 Graphs illustrating the influence of the hydraulic gradient direction ( $\lambda$ ) on (A) the pore-pressure gradient magnitude and (B) the size of the groundwater term ( $T_w$ ) normalized by the friction term ( $T_f$ ) for infinite slopes inclined at various angles,  $\theta$ . Shaded zones denote the parts of the parameter space in which groundwater effects reduce the stability of the slope. The liquefaction line applies for  $\gamma_t/\gamma_w = 2$ ; similar liquefaction lines are easily constructed for other values of  $\gamma_t/\gamma_w$  from Equations 8 and 9 (cf Iverson 1992).

circles and slope at an angle equal to the effective friction angle activated during failure by the effective normal stress,  $\sigma'_{yy}$ . At the points of tangency, the effective normal and shear stresses on failure planes (which parallel the slope surface) are given by statics:  $\sigma'_{yy} = \gamma_t y \cos \theta - p = \gamma_t z \cos^2 \theta - p$  and  $\tau_{yx} = \gamma_t y \sin \theta = \gamma_t z \sin \theta \cos \theta$ . Stresses on planes with different orientations then can be obtained from the Mohr's circle in the conventional manner (e.g. Lambe & Whitman 1979). Evaluation of these stresses leads to four important conclusions about effective stresses in failing infinite slopes: (a) The major principal effective stress,  $\sigma'_1$ , is rotated upslope from the vertical

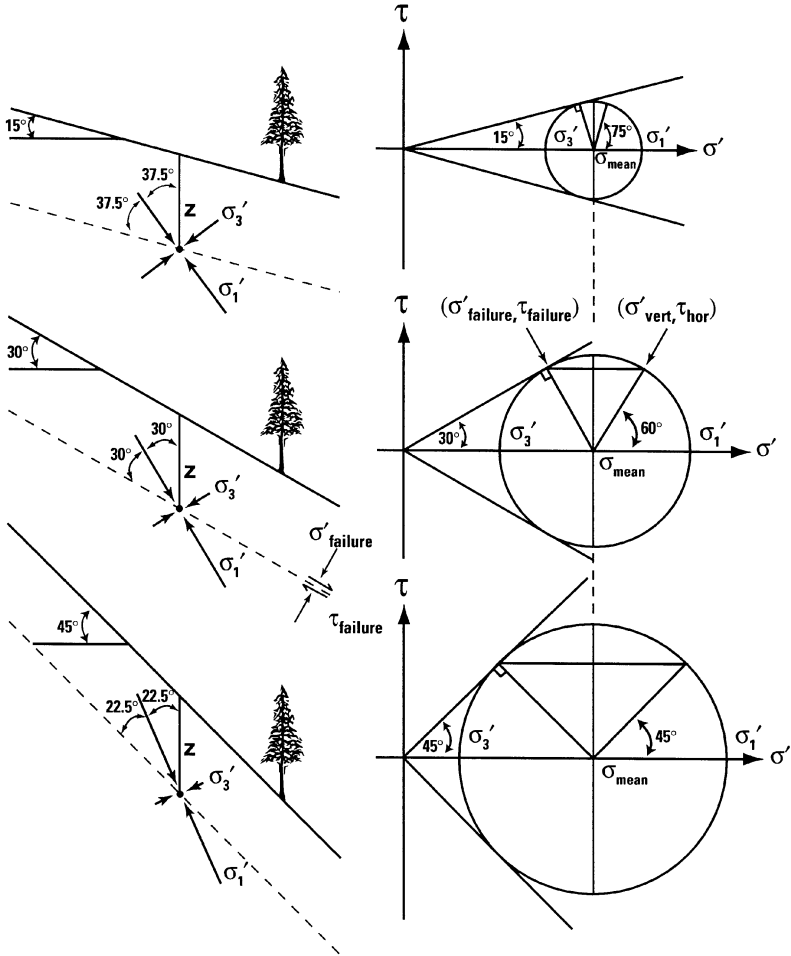


Figure 11 Effective stresses in cohesionless infinite slopes at Coulomb limiting equilibrium ( $FS = 1$ ). Diagrams on the left depict relative magnitudes and orientations of principal stresses at depth  $Z$ . Diagrams on the right show the corresponding Mohr's circles and Coulomb failure envelopes.

by an amount  $\pi/4 - \theta/2$ , and its magnitude exceeds that of the vertically oriented normal stress. (b) The vertically oriented effective normal stress,  $\sigma'_{vert}$ , exceeds the mean effective normal stress, which is necessarily geostatic,  $\sigma'_m = (\sigma'_1 + \sigma'_3)/2 = \gamma_t z - p(z)$ . (c) The effective normal stress acting on slip planes parallel to the slope,  $\sigma'_{yy} = \sigma'_{failure}$ , is less than the mean normal stress but greater than the minimum principal stress,  $\sigma'_3$ . (d) As  $\theta$  declines, the principal effective stresses become more nearly equal; in the limit  $\theta \rightarrow 0$ , the effective stress field is isotropic and the vertical effective stress is geostatic. These observations indicate that the simple liquefaction criterion given by Equation 5 applies only for virtually flat slopes, and that for steeper slopes it should be modified to account for the fact that  $\sigma'_{failure} < \sigma'_m$ . Pore pressures need only reduce  $\sigma'_{failure}$  (not  $\sigma'_m$ ) to zero in order to produce a state of zero frictional strength. Thus for failing infinite slopes (where  $\sigma_{failure} = \sigma_{yy} = \gamma_t z \cos^2 \theta$ ) the liquefaction criterion of Equation 5 may be generalized to

$$\frac{\partial p}{\partial z} = \frac{\partial \sigma_{failure}}{\partial z} = \gamma_t \cos^2 \theta. \quad (8)$$

This criterion implies that the vertical pore-pressure gradient,  $\partial p/\partial z$ , necessary to produce liquefaction decreases as the slope angle increases. For example, a flat surface requires  $\partial p/\partial z = \gamma_t$  for liquefaction, but a  $45^\circ$  slope requires a gradient of only  $\partial p/\partial z = \gamma_t/2$ , which approximates a hydrostatic gradient. Thus steep slopes can liquefy rather readily during failure if they are stable enough to become saturated with water before they fail.

If one assumes that slope-normal effective stress is responsible for resistive liquefaction, one can assess precisely the proximity of the Coulomb failure states described by Equations 7a–d to the liquefaction states described by Equation 8. This assessment determines how close a slope is to liquefying at the time of Coulomb failure, and it is facilitated by rewriting Equation 7c in terms of  $\partial p/\partial z$  by using the trigonometric relationship  $z = y/\cos \theta$  to obtain  $\partial p/\partial z = \cos \theta (\partial p/\partial y)$ . Substituting this expression in Equation 7c and combining the result with Equation 7b yields the equation

$$\frac{T_w}{T_f} = \frac{1}{\gamma_t \cos^2 \theta} \left[ \frac{d}{Y} - 1 \right] \frac{\partial p}{\partial z}. \quad (9)$$

An important special case of this equation exists for saturated slopes, with  $d = 0$ . In this case, Equation 9 reduces to  $T_w/T_f = -(1/\gamma_t \cos^2 \theta) (\partial p/\partial z)$ , which in conjunction with Equation 8 shows that  $T_w/T_f = -1$  or  $T_w + T_f = 0$  when liquefaction occurs. In contrast,  $T_w + T_f = 1$  for Coulomb failure of the same saturated slope if cohesion is absent. Thus in cohesionless infinite slopes in which  $\partial p/\partial z$  increases with time, Coulomb failure preempts liquefaction. The difference between the stress state at Coulomb failure and that required for

liquefaction can be assessed from families of graphs like those in Figure 10. In particular, Figure 10B includes a *liquefaction line* for cases in which  $\gamma_t/\gamma_w = 2$ , a condition approximated closely in many soils. In such soils liquefaction can occur only if  $(\gamma_t/\gamma_w)(T_w/T_f) \leq -2$  is satisfied. Consider, for example, the special case of a saturated slope with  $\gamma_t/\gamma_w = 2$  and slope-parallel seepage ( $\lambda = 90^\circ$ ). Figure 10B shows that  $(\gamma_t/\gamma_w)(T_w/T_f) = -1$  in this instance, which implies that Coulomb failure will occur if  $T_f = 2$  (which requires  $\phi \sim 2\theta$ ) and that the vertical pore-pressure gradient ( $\partial p/\partial z$ ) at failure is only half that required to liquefy the soil.

Cohesion may profoundly influence the state of stress necessary for Coulomb failure and the potential for subsequent liquefaction—particularly for failures at shallow depths. For saturated slopes, this influence can be seen readily from the relationships  $T_f + T_w = 0$  for liquefaction and  $FS = T_f + T_w + T_c = 1$  for Coulomb failure. Taken together, these relationships show that if  $T_c = 1$  at failure, then the pore-pressure distribution represented by  $T_w$  can liquefy the slope if cohesion breaks down during failure. For example, Equation 7d shows that  $T_c = 1$  implies  $c \approx 10$  kPa for a 1-m thick landslide on a  $30^\circ$  slope. Cohesions of approximately 10 kPa can be imparted by the strength of tree roots (Ziemer 1981, Greenway 1987) or soil cementation (Mitchell 1976). Thus pore pressures that induce Coulomb failure of soils with significant cohesion can liquefy those soils if the cohesive bonds are broken. Soils that are stabilized chiefly by tree roots on steep slopes, for example, may be quite prone to post-failure liquefaction. Root strength or other cohesion may be disrupted by agitation (i.e. development of granular temperature) that accompanies the dynamics of debris sliding on steep, rough slopes.

### *Dynamics of Sliding*

The dynamic counterpart of the static infinite-slope analysis is the rigid-body sliding model first presented by Heim (1932). Many authors have used this model to investigate landslide and debris-flow dynamics, and some have devised variations of the model that include facets of more realistic physics (e.g. Pariseau 1980, Hungr et al 1984, Hutchinson 1986, Sassa 1987, Cannon & Savage 1988, Van Gassen & Cruden 1989). However, owing to a relative lack of data for rigorous model tests, slide dynamics models remain immature compared to slope failure models. The slide dynamics model we describe below provides rudimentary insights into how changes in pore pressure and granular temperature during sliding may influence debris-flow mobilization.

Rigid-body sliding analyses assume that net downslope displacement occurs along a discrete surface at the base of the moving mass, just as in the infinite-slope model for failure of slopes with cohesion. The basic equation for rigid-body sliding employs Newton's second law of motion, which determines

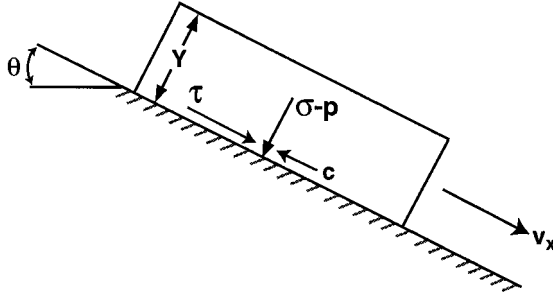


Figure 12 Definition of parameters for the rigid-body model of landslide motion.

the downslope velocity,  $v_x$ , of the slide mass as a function of time,  $t$ , (Figure 12):

$$(\gamma_t/g)Y(dv_x/dt) = \tau - (\sigma - p) \tan \phi - c. \quad (10)$$

The lefthand side of Equation 10 is the product of the downslope acceleration  $dv_x/dt$  and the mass of the sliding body per unit of slip-surface area; the righthand side describes the sum of driving and resisting stresses acting on the slip surface, as characterized by the Coulomb rule (Equation 1). The righthand side of Equation 10 implies that downslope acceleration occurs only if  $\tau > (\sigma - p) \tan \phi + c$ . In contrast, the Coulomb rule mandates that  $\tau = (\sigma - p) \tan \phi + c$ . Indeed, slip velocities implied by the Coulomb rule are indeterminate, for any  $v_x$  can satisfy Equation 10 if  $\tau = (\sigma - p) \tan \phi + c$  and steady slip occurs. Consequently, a tacit assumption in sliding models such as Equation 10 is that minor changes in  $\tau$ ,  $\sigma$ ,  $p$ ,  $\phi$ , or  $c$  during failure allow the driving stress  $\tau$  to exceed the Coulomb resistance by at least an infinitesimal amount. Such changes may result from stress-field rotation during failure (Anderson & Sitar 1995), breakdown of cohesion, changes in grain interlocking that reduce the effective value of  $\phi$ , or increases in pore pressure associated with soil contraction (Figure 4). These changes need only be slight and transitory, and need not mobilize the sliding mass into a debris flow.

Several useful variations of the basic equation of motion (Equation 10) exist. One variation results from substituting the expressions for stresses acting at the base of infinite slopes,  $\tau = \gamma_t Y \sin \theta$  and  $\sigma = \gamma_t Y \cos \theta$ , and then dividing all terms by  $\gamma_t Y$ . These operations yield

$$\frac{1}{g} \frac{dv_x}{dt} = \sin \theta - \cos \theta \tan \phi + \frac{p(Y)}{\gamma_t Y} \tan \phi - \frac{c}{\gamma_t Y}, \quad (11)$$

where  $p(Y)$  denotes that  $p$  is the pore pressure at depth  $Y$ . The rigid-body model described by Equation 11 forms the nucleus of more general models that

account for the evolving shape of a landslide or debris-flow mass as it simultaneously undergoes pervasive Coulomb failure and downslope motion (Iverson & LaHusen 1993, Hungr 1995, Iverson 1997). In these more general models, the distribution of pore pressure  $p(x,y,t)$  plays a critical role in determining the mobility of the mass (Iverson 1997). In the rigid-body model governed by Equation 11, in contrast, the effects of pore pressure are restricted to those of the basal pore pressure,  $p(Y)$ . This difference simplifies analysis of rigid-body models but also underscores their limitations.

An alternative form of Equation 11 provides additional insight into the connections among slope failure, downslope motion, and debris-flow mobilization. The alternative form can be obtained by substituting in Equation 11 the expressions given in the limit-equilibrium equations (7a-d) and making the identification in Equation 7c that  $p(Y)/Y = [(d/Y) - 1](\partial p/\partial y)$  (which may be demonstrated formally by integrating the pore-pressure distribution from  $y = 0$  to  $y = Y$ ). These operations produce

$$\begin{aligned} dv_x/dt &= g \sin \theta (1 - T_f - T_w - T_c) \\ &= g \sin \theta (1 - FS). \end{aligned} \quad (12)$$

This equation shows clearly how reductions in  $FS$  that accompany slope failure can enhance acceleration of the mass. However, Equation 12 does not explicitly include mechanisms by which such reductions might occur.

Changes in soil agitation (granular temperature) that may influence  $FS$  can be incorporated in an elementary way by rewriting Equation 12 as an energy-conservation equation. The first step involves multiplying each side of the equation by  $v_x$  and recognizing that  $v_x(dv_x/dt) = \frac{1}{2}[d(v_x^2)/dt]$  is the rate of change of translational kinetic energy per unit mass of the sliding body. This yields

$$\frac{1}{2}[d(v_x^2)/dt] = v_x g \sin \theta (1 - FS). \quad (13)$$

On the righthand side of Equation 13,  $v_x g \sin \theta$  is the rate of potential energy loss per unit mass by the sliding body as it descends the slope, and  $-v_x g \sin \theta (FS)$  is the rate of frictional energy dissipation per unit mass. Thus the righthand side of Equation 13 represents the net energy available, per unit mass, for conversion to kinetic energy. An assumption implicit in Equation 13 is that all kinetic energy generated by descent of the sliding mass appears as translational kinetic energy. For landslides and debris flows this is a poor assumption, for translation of the moving mass along a rough surface must cause some energy to transform to internal energy manifested as grain vibrations. The net conversion of translational kinetic energy to vibrational kinetic energy per unit mass may

be represented by  $\langle \frac{1}{2} \psi^2 \rangle$ , where  $\psi$  has dimensions of velocity and describes production of velocity fluctuations  $v'$  owing to interaction of slip-surface grains with the rough bed, as illustrated in Figure 5 (Iverson 1997). The rough bed can dampen velocity fluctuations as well as produce them, and  $\psi$  is the net rate of production after the dampening effects of Coulomb friction (indicated by  $FS > 0$ ) are subtracted. Granular temperature,  $T$ , depends on  $\langle \frac{1}{2} \psi^2 \rangle$  and on the inelasticity of grain collisions with the bed. A steady sliding model that neglects viscous dissipation by pore fluid predicts that granular temperature is an explicit function of  $\langle \frac{1}{2} \psi^2 \rangle$  (Iverson 1997), given by

$$T = \frac{8 \langle \frac{1}{2} \psi^2 \rangle e^2}{(1 - e)^2 (1 + e)^4}. \quad (14)$$

Here  $e$  is the coefficient of restitution for grain collisions;  $e = 1$  for perfectly elastic collisions, but  $e \rightarrow 0$  as collisions approach complete inelasticity. As  $e \rightarrow 1$ ,  $T \rightarrow \infty$  unless  $\langle \frac{1}{2} \psi^2 \rangle = 0$  and frictional dissipation balances production of vibrational energy. For typical sediment grains,  $e \sim 0.1$  may be more representative, and granular temperature is therefore finite even when  $\langle \frac{1}{2} \psi^2 \rangle$  is positive.

Landslide potential energy converted to vibrational kinetic energy is unavailable for performing translational work—at least in the simplest case, which excludes the possibility of feedback between vibration and downslope motion. To account for production of vibrational kinetic energy, Equation 13 must be generalized to

$$\frac{1}{2} [d(v_x^2)/dt] + d \left\langle \frac{1}{2} \psi^2 \right\rangle / dt = v_x g \sin \theta (1 - FS). \quad (15)$$

This equation provides a basis for constraining how much vibrational energy may be available to break cohesive bonds and assist debris-flow mobilization. In an extreme case, all kinetic energy produced by descent of the moving mass is converted to vibrational kinetic energy. Then the downslope velocity  $v_x$  is constant and Equation 15 reduces to a simple differential equation with  $\langle \frac{1}{2} \psi^2 \rangle$  as the only dependent variable.

With  $v_x$  constant in Equation 15, the quantity  $\langle \frac{1}{2} \psi^2 \rangle$  characterizes the maximum net production of vibrational kinetic energy per unit mass, whereas vibrational kinetic energy per unit volume determines the energy density available for generating local stresses that might break cohesive bonds. Assuming  $v_x$  is constant, multiplying each side of Equation 15 by the total bulk density of the moving mass,  $\rho_t$ , yields an equation for the maximum volumetric density of vibrational kinetic energy,  $\rho_t \langle \frac{1}{2} \psi^2 \rangle$ , which can be solved easily. Use of the initial condition  $\langle \frac{1}{2} \psi^2 \rangle = 0$  at  $t = 0$  and the substitution  $H = v_x t \sin \theta$  in this

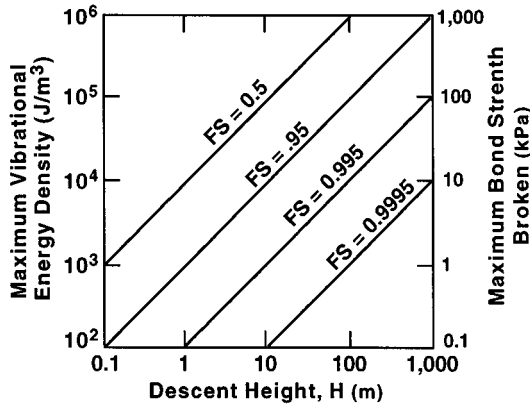


Figure 13 Plot of Equation 16, which describes the maximum vibrational energy density generated by moving landslides with differing factors of safety ( $FS$ ) during descents of vertical distance  $H$ . The vibrational energy density can be equated with the strength of cohesive bonds that may be broken by vibration. Plotted lines assume  $\gamma_t = 20,000 \text{ N/m}^3$ , which is a good approximation for many landslides.

solution yields

$$\rho_t \left\langle \frac{1}{2} \psi^2 \right\rangle = \gamma_t H (1 - FS), \tag{16}$$

where  $H$  is the vertical distance of landslide descent in a unit of time. Equation 16 indicates that the maximum vibrational kinetic energy density available to agitate a landslide mass descending at a constant rate depends only on  $H$ ,  $\gamma_t$ , and  $1 - FS$ . For most landslides and debris flows a reasonable estimate is  $\gamma_t = 20,000 \text{ N/m}^3$ , and Figure 13 depicts a plot of Equation 16 for this value of  $\gamma_t$ . According to the figure, if  $FS = 0.95$ , for example, a landslide descent of 1 m could at most produce an energy density sufficient to break cohesive bonds with a strength of 1 kPa. A descent of at least 10 m would be required to generate the energy density to break bonds of 10 kPa. This dynamic breakdown of soil cohesion by vibration due to downslope motion appears plausible, but it depends sensitively on  $FS$ .

If a descending landslide becomes at least partly liquefied,  $FS \ll 1$  is possible, and according to Figure 13, reduction of  $FS$  greatly enhances the vibrational kinetic energy that may be available to break cohesive bonds. This effect points to the existence of a feedback process that can favor debris-flow mobilization: If pore pressures rise during Coulomb slope failure (for example, as a result of soil contraction),  $FS$  declines and production of kinetic energy increases. Then more energy is available to agitate the moving mass, break down cohesion, and

further reduce  $FS$ . Mathematical analysis of this feedback process is beyond the scope of this review but suggests that the process can become unstable and actuate the transition from rigid landslide to mobilized debris flow.

### *Pore Pressure Generation During Slope Failure and Sliding*

If pore pressures that change during slope failure can modify  $FS$  and instigate feedback that favors debris-flow mobilization, what controls the pore-pressure changes themselves? For infinite slopes, coupling between landslide motion and pore-pressure changes can be analyzed with a one-dimensional, quasistatic pore-pressure diffusion model (e.g. Hutchinson 1986). The model predicts that pore pressures may increase in response to monotonic contractive strains of the granular matrix in the  $y$  direction and decrease in response to monotonic dilative strains. A more complicated but fundamentally similar model applies if soil deformation involves significant inertial forces and large displacements of the solid grains that produce sequential contraction and dilation (Iverson 1993). In all cases the key issue entails the relative time scales for generation and dissipation of pore-pressure deviations from equilibrium values. The factors that control these time scales can influence the propensity for debris-flow mobilization.

The basic elements of one-dimensional, quasistatic pore-pressure diffusion models, also known as soil consolidation models, have been detailed by many authors (e.g. Bear 1972, Lambe & Whitman 1979). In Appendix 1 we list the elements to highlight key assumptions. In summary, such models assume that the  $y$ -direction compressive strain  $\epsilon_{yy}$  results exclusively from pore-volume change, that  $\epsilon_{yy}$  is proportional to effective stress,  $\sigma'_{yy} = E\epsilon_{yy}$ , and that  $\epsilon_{yy}$  is small, which yields  $\dot{\epsilon}_{yy} = \partial v_y / \partial y$ , where the overdot denotes the partial time derivative. These assumptions, together with Darcy's law for pore-fluid flow, lead to the pore-pressure diffusion equation:

$$\frac{\partial p'}{\partial t} = \frac{KE}{\rho_w g} \frac{\partial^2 p'}{\partial y^2}, \quad (17)$$

in which  $p'$  is the nonequilibrium (unsteady) component of pore pressure and  $\rho_w$  is the density of the pore water. If the steady background pore-pressure distribution is hydrostatic, the nonequilibrium pore pressure is related to the hydraulic head by  $p' = \rho_w gh$ , but this need not be true in slopes. The stress-strain proportionality constant,  $E$ , can be regarded as an elastic stiffness (Young's) modulus or reciprocal compressibility of the granular matrix. The coefficient  $KE/\rho_w g$  serves as the hydraulic diffusivity; it can be written in the equivalent form  $kE/\mu$ , where  $k$  is the intrinsic hydraulic permeability of the granular matrix and  $\mu$  is the viscosity of the pore water, and this form is employed below.

A more useful version of Equation 17 results from normalizing it by introducing dimensionless variables defined as  $p'^* = p'/\rho_w gY$ ,  $y^* = y/Y$ , and

$t^* = t\dot{\epsilon}_{yy}$ . These normalizations employ a fundamental length scale of  $Y$  and time scale of  $1/\dot{\epsilon}_{yy}$ . Inserting the dimensionless variables in Equation 17 yields

$$\frac{\partial p^*}{\partial t^*} = \frac{t_{def}}{t_{diff}} \frac{\partial^2 p^*}{\partial y^{*2}}. \quad (18)$$

In this equation,  $t_{def}/t_{diff} = (kE)/(Y^2\mu\dot{\epsilon}_{yy})$  is the nondimensional hydraulic diffusivity, which expresses the ratio of the time scale for pore deformation,  $t_{def} = 1/\dot{\epsilon}_{yy}$ , to the time scale for pore-pressure diffusion,  $t_{diff} = (Y^2\mu)/(kE)$ . Solutions of the diffusion equation (e.g. Carslaw & Jaeger 1959) show that  $t_{def}/t_{diff}$  determines the extent to which nonequilibrium pore pressures resulting from soil volume change can develop and persevere. The limit  $t_{def}/t_{diff} \rightarrow 0$  represents a perfectly undrained condition with total transfer of solid stress to nonequilibrium pore pressure, whereas the limit  $t_{def}/t_{diff} \rightarrow \infty$  represents a perfectly drained condition without development of nonequilibrium pore pressure. Soil deformation during slope failures generally falls between these extremes.

To estimate the degree to which soil volume change produces nonequilibrium pore pressures, the value of  $t_{def}/t_{diff}$  must be estimated. During the first stages of soil deformation, prior to attainment of critical-state density, the characteristic value of  $\dot{\epsilon}_{yy}$  scales with the depth-averaged shear-strain rate defined by  $v_x/Y$ . Thus  $t_{def} \sim Y/v_x$  and  $t_{def}/t_{diff} \sim (kE)/(Y\mu v_x)$  (cf Rudnicki 1984, Iverson & LaHusen 1989). Employing this estimate as a basis for calculation, consider, for example, hypothetical 1-m thick landslides initially moving at rates ranging from  $10^{-4}$  m/s to 10 m/s. For such landslides Figure 14 shows plots of values of  $t_{def}/t_{diff}$  calculated using a range of hydraulic diffusivities typical of diverse soils (cf Roeloffs 1996, Iverson 1997). The trends depicted in Figure 14 illustrate a key point:  $t_{def}/t_{diff}$  can be  $\gg 1$  or  $\ll 1$  for both coarse- and fine-grained soils, depending on the rate of landslide motion and soil deformation. For example, if downslope motion exceeds 1 m/s during failure, even coarse soils may mimic undrained behavior, and high pore pressures may develop as a result of soil contraction. Conversely, fine-grained soils may exhibit drained behavior without significant pore-pressure change if landslide motion is sufficiently slow. Lack of pore-pressure change decreases the propensity for debris-flow mobilization during contractive soil failure, but it enhances the propensity for mobilization if failure involves soil dilation, for it inhibits development of negative pore pressures (suction) that may transiently strengthen the soil (Rice 1975). In summary, no unequivocal rule describes the tendency for various soils or landslides to develop high or low pore pressures during failure. The behavior depends on the ratio  $t_{def}/t_{diff}$  as well as on the initial soil density.

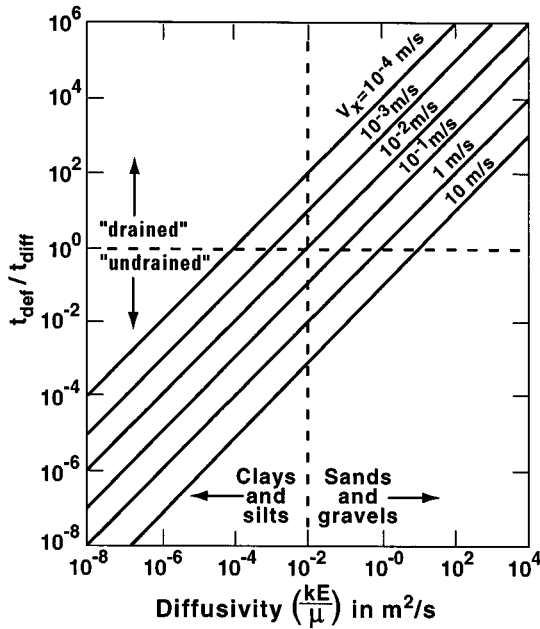


Figure 14 Values of  $t_{def}/t_{diff}$  plotted as a function of the hydraulic diffusivity,  $kE/\mu$ , for various values of the downslope landslide speed,  $v_x$ . All plots assume a landslide thickness,  $Y$ , of 1 m; comparable sets of plots are easily obtained for other landslide thicknesses. For reference, dashed lines distinguish ranges of hydraulic diffusivities that commonly characterize different soil types and ranges of  $t_{def}/t_{diff}$  that, in the limit, approach drained and undrained behavior.

## FAILURE AND MOBILIZATION OF TWO-DIMENSIONAL SLOPES

The mathematical idealizations of infinite-slope analyses provide important insights, but they lead to predictions that are untestable, because no physical slope is one-dimensional. In this section we consider two-dimensional slopes in which physical quantities can vary in both the slope-parallel and slope-normal directions. Two-dimensional slopes exhibit many of the complexities of three-dimensional slopes, including static indeterminacy of stresses. More important, two-dimensional slopes can be simulated well in physical experiments, which yield data crucial for testing hypotheses and models. No field study has yet obtained high-resolution data for a debris-flow mobilization event—despite much effort devoted to detailed monitoring and manipulation of field sites (e.g. Wilson & Dietrich 1987, Harp et al 1990, Johnson & Sitar 1990, Montgomery et al

1990). Consequently, we describe here the results of controlled laboratory experiments and ancillary modeling that yield a two-dimensional picture of debris-flow mobilization that is more complete than has been afforded by field data.

Several investigators have performed laboratory experiments in which the geometry and boundary conditions of a failing soil mass approximated conditions in two-dimensional slopes (e.g. Fukuzono 1985, Iverson & LaHusen 1989, Eckersley 1990). The design of these experiments permitted relatively limited downslope displacements, however, because the artificial landslides moved directly onto flat runout surfaces and stopped. This prevented observations and measurements of the complete debris-flow mobilization process. Here we focus on a pair of experiments conducted in June 1995, at the US Geological Survey (USGS) debris-flow flume (Iverson et al 1992, Iverson 1997), which permitted full mobilization and unrestricted runout. The configurations of the two experiments were nearly identical except for subtle differences in the groundwater regimes that triggered slope failure and in pre-failure soil bulk densities. These subtleties produced important differences in the styles of slope failure and debris-flow mobilization. We identify the differing styles as mode I and mode II mobilization. Inspection of debris-flow sites in the field (e.g. Ellen et al 1988) provides qualitative corroborating evidence for the occurrence of these distinctive modes.

### *Methods and Materials*

We conducted the two experiments (designated I and II hereafter) in the USGS debris-flow flume, a 95-m long, 2-m wide concrete chute with a 31° slope, roughened bed, and smooth side walls (Iverson et al 1992). In each experiment we formed a tabular prism of 6.1 to 6.4 m<sup>3</sup> of moist, granular soil by dumping and shoveling it behind a rigid, 0.65-m-high retaining wall installed near the head of the flume (Figure 15). We performed no systematic densification of the soil. The basic procedure in each experiment involved adding water to the soil prism until slope failure occurred and a debris flow mobilized. We anticipated that chances for mobilization were good owing to the steepness of the slope, the looseness of the soil, and the high soil water content expected at the time of failure.

Table 2 summarizes results of laboratory analyses of soil properties. Desiccated samples of the soil consisted of about 60% poorly sorted sand and 40% fine (<10 mm) gravel by weight. At the time of placement in the flume, the soil had engineering water contents (weight of water ÷ weight of solids) ranging from 0.08 to 0.09 and volumetric water contents ranging from about 15 to 20%. Grab samples of the surface soil and in situ measurements with an array of subsurface time-domain reflectometry (TDR) probes developed by Herkelrath et al (1991) yielded similar values for average water contents, although the TDR probes revealed more spatial heterogeneity than did grab

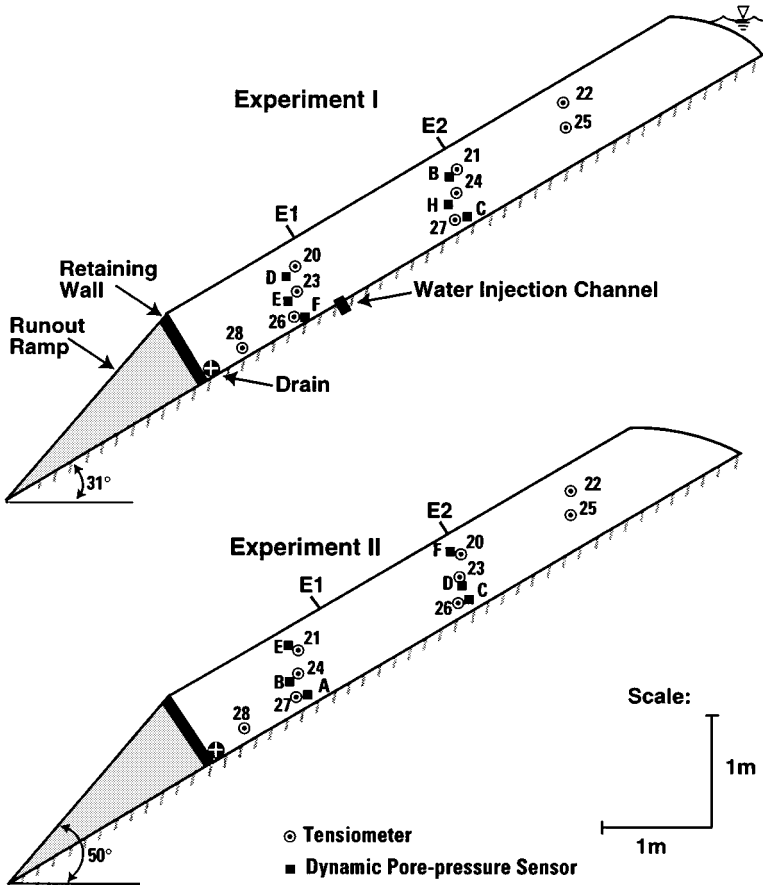


Figure 15 Schematic profiles of soil prisms used in debris-flow mobilization experiments I and II. Numbers identify tensiometers. Letters identify dynamic pore-pressure sensors. E1 and E2 identify anchor points for extensometers 1 and 2. The concrete flume bed extends 85 m downslope beyond the runout ramp.

sampling. Bulk-density samples obtained using Blake’s (1965) excavation method near the surface of the loaded soil yielded mean dried bulk densities of 1400 kg/m<sup>3</sup> in experiment I and 1600 kg/m<sup>3</sup> in experiment II. From these data we inferred mean porosities of about 0.48 in experiment I and 0.41 in experiment II. The difference in soil porosity between experiments apparently resulted from greater compaction by random foot traffic during soil loading in experiment II. In both experiments slight but unmeasured additional compaction of the soil occurred during subsequent application of water.

We measured the friction angle between the soil and concrete flume bed by placing dried 30-kg soil samples on a horizontal concrete slab textured like the flume bed. We gradually tilted the slab upward until sliding occurred at the soil-concrete interface. Numerous replicates yielded a basal friction angle  $\phi_{base}$  of  $30^\circ$ . We measured the internal friction angle of the dried soil using comparable tilting-slab tests modified so that slip barriers forced the soil to fail internally (Lill 1993) and by conventional triaxial compression tests under confining stresses of 70 and 140 kPa. Both types of tests yielded  $\phi = 40^\circ$ . The triaxial tests yielded a cohesion of zero and uniaxial (secant) compression moduli of  $E = 1.7 \times 10^7$  Pa at 70 kPa load and  $E = 4.8 \times 10^7$  Pa at 140 kPa load. Constant-head permeameter tests on loosely packed soil specimens yielded  $k \sim 10^{-10}$  m<sup>2</sup> ( $K \sim 10^{-3}$  m/s), but additional permeameter tests with similar soil showed that  $k$  can vary by nearly two orders of magnitude depending on the degree of soil compaction (Iverson 1997, Major 1996). Combined with the other pertinent parameters,  $k = 10^{-10}$  yielded a pore-pressure diffusion time scale  $t_{diff} \sim 0.2$  s, but values of 2 s or even 20 s appeared plausible given that soil densification could accompany slope failure (Iverson 1997).

In addition to the network of six TDR probes, instrumentation used in each experiment included nine tensiometers equipped with bidirectional pressure transducers (Baum & Reid 1995), six custom-built pore-pressure sensors designed for optimal dynamic response (Iverson & LaHusen 1989), and two extensometers to measure soil-surface displacement. Positions and labels of sensors varied slightly between experiments (Figure 15). The dynamic pore-pressure sensors were equipped with thin, flexible cables that enabled them to travel roughly 5 m downslope with the moving soil while imparting minimal disturbance. In addition, an automated laser distance-ranging system and basal normal-load cell were positioned 2 m downslope from the retaining wall to measure the thickness and bulk density of mobilized debris flows as they passed (cf Iverson 1996). Data from all sensors were logged digitally with a personal computer equipped with hardware and software for high-speed, high-volume data acquisition. Tensiometer and extensometer data were logged at 1 Hz for the duration of each experiment. During slope failure and flow mobilization, pore-pressure, displacement, flow-depth, and basal stress data were logged at 1000 Hz.

The chief procedural difference between experiments I and II was the method of water application. In experiment I, all water was added as groundwater by a subsurface conduit in the flume bed 1.2 m upslope from the retaining wall and an infiltration pond at the upslope end of the soil prism. This arrangement simulated a hydrologic state in which groundwater percolation dominates water

**Table 2** Material properties and volumetric water budgets for debris-flow mobilization experiments I and II

	Experiment I*	Experiment II*
Material properties		
Initial water content (weight water/weight solids)	0.08–0.09	0.08–0.09
Dried bulk density (kg/m <sup>3</sup> )	1340–1430	1480–1630
Mean porosity (computed from bulk densities)	0.48	0.41
Internal friction angle, $\phi$ (degrees)	40	40
Basal friction angle, $\phi_{base}$ (degrees)	30	30
Hydraulic permeability, $k$ (m <sup>2</sup> )	$\sim 10^{-10}$	$\sim 10^{-10}$
Young's modulus, $E$ (Pa)	$\sim 10^7$	$\sim 10^7$
Volumetric water budget		
Soil volume (m <sup>3</sup> )	6.4	6.1
Total pore space (m <sup>3</sup> )	3.1	2.5
Pore space filled by initial moisture** (m <sup>3</sup> )	0.7–1.7	0.8–1.2
Water applied (m <sup>3</sup> )	1.1	1.8
Water discharged from drain (m <sup>3</sup> )	0.1	0.5
Water loss to wind deflection and spray evaporation (m <sup>3</sup> )	0	0.2***
Net water added (m <sup>3</sup> )	1.0	1.1
Water in soil at failure (m <sup>3</sup> )	1.7–2.7	1.9–2.3
Percent saturation of pore space at failure	55–85%	76–92%

\*Where a range of values is listed, the range expresses the minimum and maximum values measured or calculated on the basis of spatially variable data.

\*\*TDR probes indicated that initial soil moisture content was considerably more heterogeneous in experiment I than in experiment II.

\*\*\*Water loss to wind deflection and spray evaporation was estimated by measuring the mean rainfall reaching the soil surface with four rain gauges and computing the total volume of rainfall reaching the soil surface (0.191 m rainfall measured  $\times$  8.4 m<sup>2</sup> soil area = 1.6 m<sup>3</sup> rainfall volume). Subtraction of this value from the total water applied (1.8 m<sup>3</sup>) yields the water-loss estimate.

inflow to the slope. In experiment II, all water was added by surface sprinkling from a set of nozzles that simulated rainfall at an average rate of 5 cm/h. In each experiment, a horizontal drain pipe positioned against the base of the retaining wall and equipped with a control valve allowed us to monitor and manipulate groundwater discharge from the lower end of the soil prism. This, in addition to detailed metering of water input, allowed us to construct a water balance for each experiment. Table 2 summarizes the water-balance data.

Figures 16 and 17 show the pore-pressure and displacement data collected prior to and during slope failure in experiments I and II. Figure 15 depicts the locations of sensors identified by letters and numbers in Figures 16 and 17. Figure 18 shows examples from sequences of still photographs taken of the failing and mobilizing soil masses. Videotape recordings allowed us to time-register these photographs and interpolate between them.

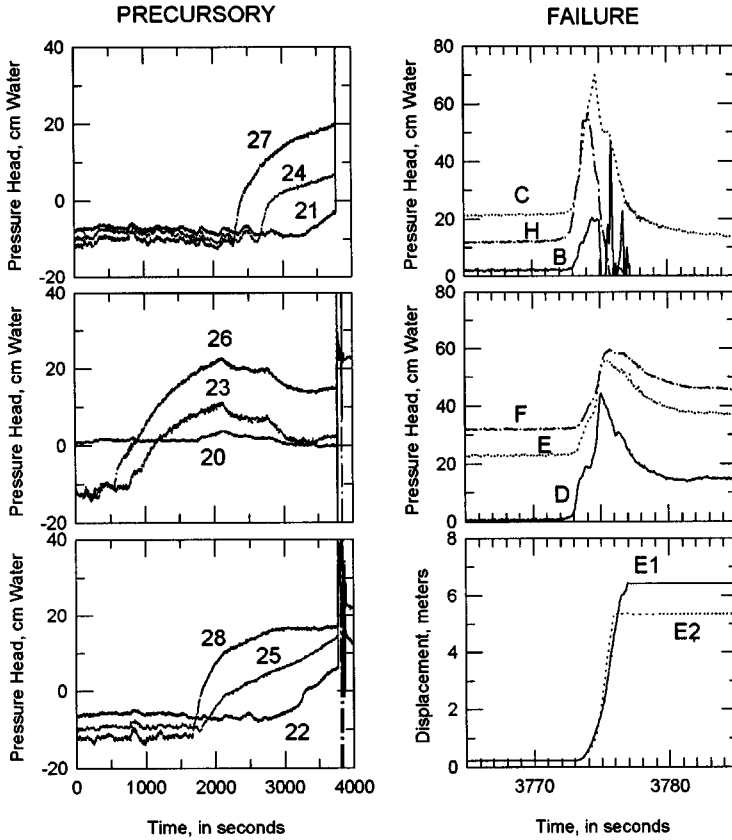


Figure 16 Data for experiment I (water application as groundwater). Identification of sensors by number or letter is keyed to Figure 15. Plots in the left column show pore pressures (expressed in units of water head) for the experiment duration up to the time of failure. Plots on the right show pore pressures and ground-surface displacements for a 20-second interval centered on the time of slope failure.

*Experiment I: Mode I Mobilization*

Application of water exclusively by subsurface flow resulted in the behavior summarized in Figure 16. Initially, negative pore pressures (suctions) existed everywhere within the soil (except, possibly, in the vicinity of tensiometer 20). Pore pressures first became positive in the vicinity of tensiometers 23 and 26, which were located near the groundwater-feed conduit. Positive pore pressures developed most slowly in the vicinity of tensiometers 21, 24, and 27, which were positioned between the upslope infiltration pond and downslope

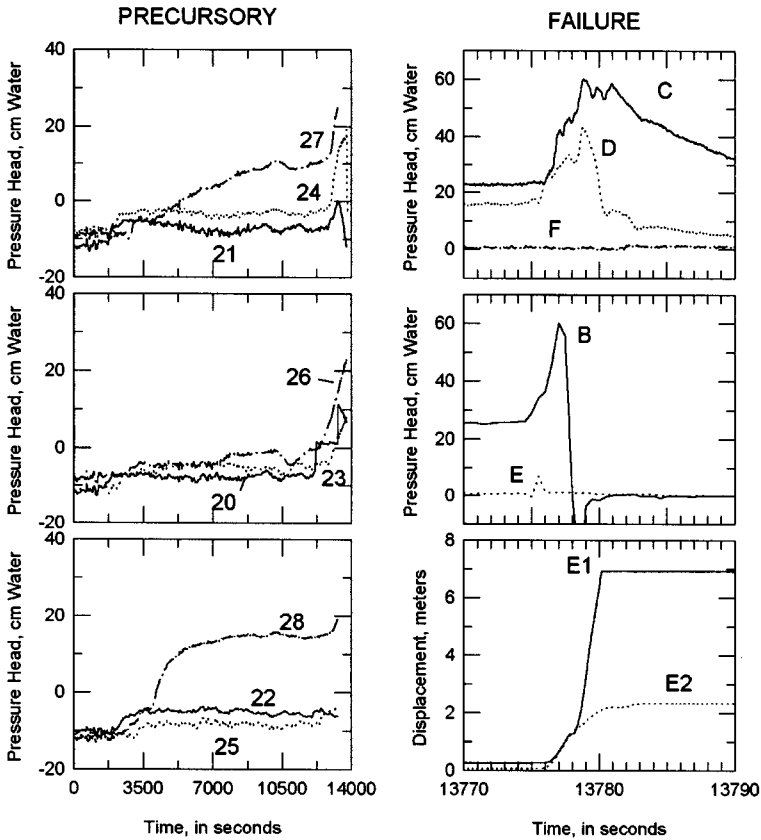
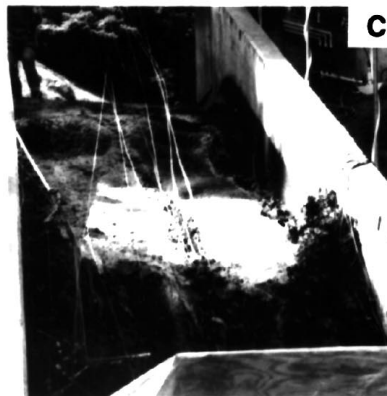
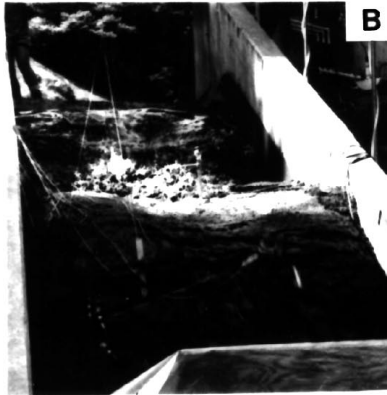
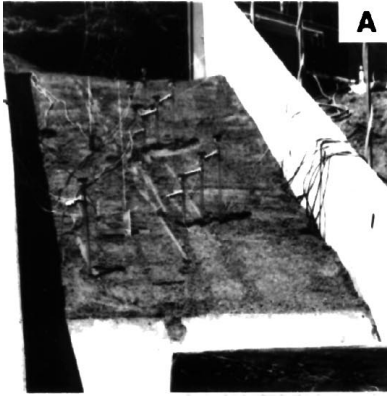


Figure 17 Data for experiment II (water application by sprinkling). Identification of sensors by number or letter is keyed to Figure 15. Plots in the left column show pore pressures (expressed in units of water head) for the experiment duration up to the time of failure. Plots on the right show pore pressures and ground-surface displacements for a 20-second interval centered on the time of slope failure.

groundwater-feed conduit. In all locations positive pore pressures developed soonest at the greatest depths, indicating a rising water table. To establish a uniform water table we decreased the inflow to the downslope conduit at about  $t = 2000$  s. Consequently, pore pressures measured by tensiometers 23 and 26 began to decline somewhat as pore pressures elsewhere continued to rise. At about this time we also opened the drain pipe positioned against the base of the retaining wall. In this manner, after about 1 h (3600 s) of water application, the soil developed a nearly uniform water table 20–30 cm beneath the surface

## EXPERIMENT I



## EXPERIMENT II

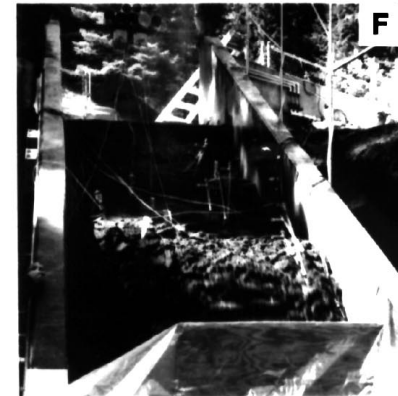
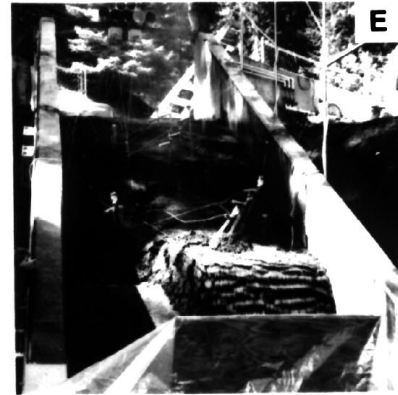
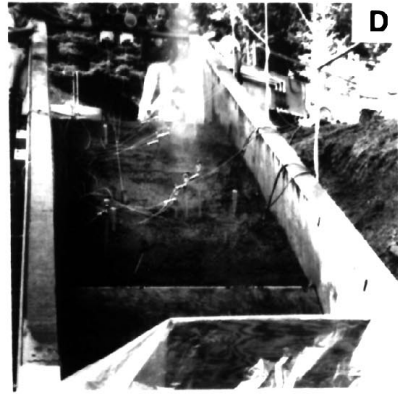


*Figure 18* Photographs of mobilization of experimental debris flows. *A*, *B*, and *C* show experiment I. *D*, *E*, and *F* show experiment II. In each sequence the first photo shows the slope prior to failure, the second photo shows the slope about 1 s after failure commenced, and the third photo shows the slope about 3 s after failure commenced.

(Figure 19A). Some upward-directed seepage and slight groundwater exfiltration was apparent at the toe of the slope, but overall the situation simulated quite well a state of slope-parallel groundwater flow above an impermeable substrate. TDR data showed that the volumetric moisture content in the soil above the water table increased somewhat during the experiment, apparently due to capillary rise.

Extensometers E1 and E2 each recorded about 2 cm of downslope soil creep prior to slope failure. Creep began after about 800 s of water application, contemporaneous with the initial development of a measurable water table. We consequently inferred that creep deformation began along the weak soil-concrete interface rather than within the soil. Prior to failure, we measured no acceleration of creep comparable to that measured by Fukuzono (1985) in experimental landslides and subsequently advocated by Voight (1989) as a universal rule. Instead, creep progressed at a more-or-less constant rate until slope rupture occurred abruptly at  $t = 3773$  s (Figure 16).

The right half of Figure 16 depicts the conspicuous soil acceleration and dynamic pore-pressure responses that occurred during slope failure. The left half of Figure 18 shows photographs of the slope before failure, about 1 s after initial rupture, and about 3 s after rupture, when the soil speed had accelerated to about 2 m/s. The soil appeared to liquefy almost spontaneously, within one or two seconds of failure, and dynamic pore-pressure data confirmed this observation. Pore-pressure sensors in two nests (C, H, B and F, E, D) all recorded rapid, dramatic pore-pressure growth contemporaneous with the rapid soil displacement that began at  $t = 3773$  s. Pore pressures at all locations more than doubled during failure, similar to behavior measured by Iverson & LaHusen (1989) and by Eckersley (1990). Pore pressures necessary to liquefy the soil can be estimated from Equation 8, which indicates  $\partial p/\partial z \sim 14$  kPa/m would be necessary for liquefaction in this circumstance. To satisfy this criterion, the peak pore-pressure heads depicted on the right side of Figure 16 must be about 1.4 times greater than the corresponding sensor depth. The measured peak heads range from about 1.0 to 1.4 times the corresponding sensor depth, indicating a state close to complete liquefaction. However, because the soil mass extended and thinned as it failed, the soil stress state undoubtedly differed from the static, infinite-slope state assumed in deriving Equation 8. Indeed, the large simultaneous increase in pore pressure at all depths suggests that soil agitation and contraction spread very quickly from the locus of initial slip to the surrounding soil. Figure 16 shows that after two or three seconds of rapid motion, pore pressures measured by the sensors declined as the soil thickness declined and the sensor cables pulled free from the soil. After about five to six meters of displacement, extensometer anchors also pulled free, but the soil continued to descend the flume as a debris flow.

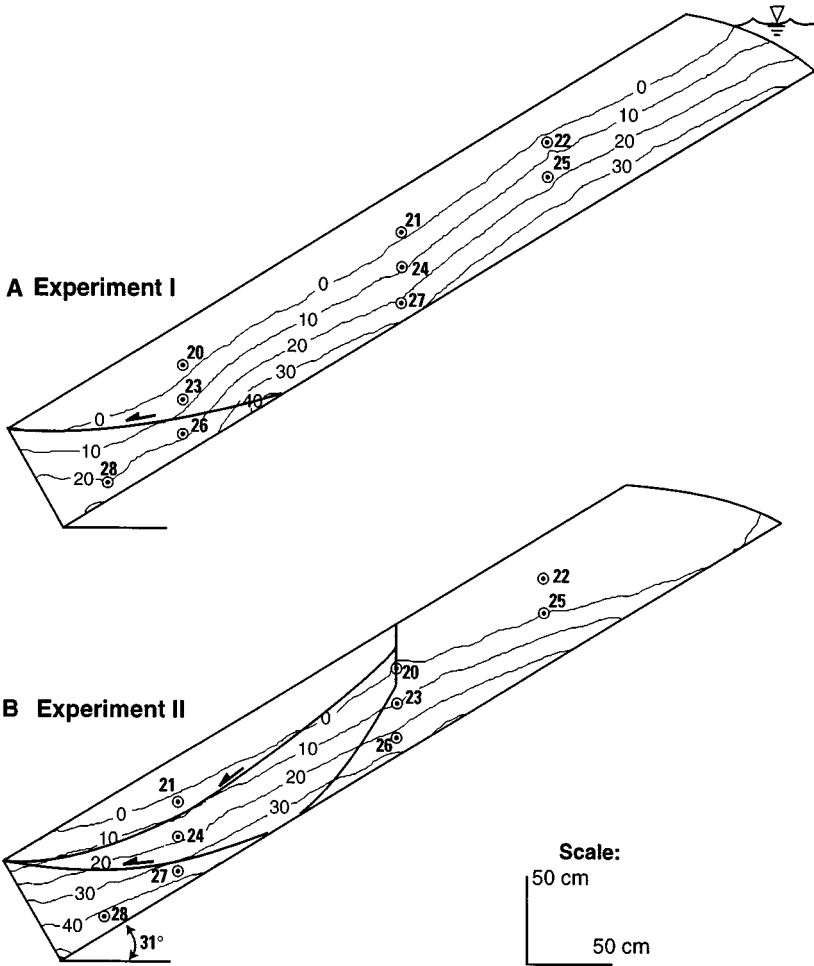


Figure 19 Pore-pressure head contours and position of failure surfaces used in Janbu limit-equilibrium analyses of slope failure. Units of pressure head are centimeters of water. Numbered circles identify positions of tensiometers, from which the pressure head data were obtained. In case B (experiment II) each of two alternative failure surfaces terminates upslope at a tension crack; the upper failure surface provides the lowest factor of safety and best mimics the shallow appearance of the initial failure.

Sensors B and D, which were positioned at or slightly above the water table, registered particularly noteworthy pore-pressure responses. When failure commenced, pore pressures measured by B and D were practically zero. Nonetheless, pore pressures at these locations increased dramatically during failure. Soil contraction apparently changed the soil from unsaturated to saturated in these locations, and the attendant increase in pore pressure produced a substantial loss of frictional strength. This flashing from a negative to positive pore-pressure state is analogous to that due to rainfall on tension-saturated soil (cf Gillham 1984), but in this instance flashing results from dynamic soil response.

Slope failure in experiment I appeared to involve almost the entire  $6.4 \text{ m}^3$  soil mass. We inferred that slip occurred first along the contact between the soil and underlying concrete, where the friction angle was  $10^\circ$  less than in the soil itself. Figure 19A illustrates the slip surface and pore-pressure distribution we used in a two-dimensional limit-equilibrium analysis of failure that employed Janbu's (1973) method of slices as implemented by Baum & Fleming (1991). We obtained contours of pore-pressure head by numerically fitting a steady-state groundwater flow solution to the tensiometer data measured just prior to slope failure. Water ponded at the top of the slope imposed a small surcharge that also affected the limit-equilibrium analysis. For this scenario, employing our independent measurements of soil density and friction angles, we computed an *FS* of 1.11. Various phenomena might explain why this *FS* deviates from the theoretical value of 1.0. Rather than speculate about these possibilities, we emphasize instead that the difference between 1.0 and 1.11 is relatively small, and that the Janbu limit-equilibrium calculation appears to explain failure adequately within the bounds of experimental error.

Although nearly the entire soil mass failed in experiment I, only about  $3.4 \text{ m}^3$  flowed over the retaining wall and down the flume. The remainder pooled behind the retaining wall as a slurry that appeared and acted liquefied when probed with a finger. After about 12 h of consolidation, we collected samples of the densified slurry that yielded a mean dried bulk density of about  $1500 \text{ kg/m}^3$ , which represents a porosity reduction of about 10% from the pre-failure state. Laser flow-depth and basal load-cell data collected downslope in the manner described by Iverson (1997) showed that the mobilized debris flow had a porosity comparable to that of the static soil, but resolution of the data was inadequate to determine whether the density was closer to the pre-failure or post-failure static density.

### *Experiment II: Mode II Mobilization*

Application of water exclusively by surface sprinkling at an average of  $5 \text{ cm/h}$  resulted in the behavior summarized in Figure 17. The hydrologic response and failure mode differed greatly from that in experiment I. TDR data showed

that a wetting front moved slowly downward from the surface, but that the soil remained unsaturated behind the wetting front. This behavior was not surprising, as the sprinkling intensity was nearly two orders of magnitude smaller than  $K$  for the loosely packed soil. The slope remained wholly unsaturated for more than an hour (3600 s), although shortly thereafter a water table began to develop near tensiometer 28 and then near tensiometer 27. Both tensiometers were located near the bed and close to the retaining wall (Figure 15). For more than three hours the saturated zone remained confined to a small wedge in this area. At  $t = 11,400$  s we doubled the sprinkling intensity. Conspicuous exfiltration, surface runoff, and development of miniature surficial debris flows ensued, indicating that raindrop impact and infiltration had altered the loose structure of the surface soil and significantly reduced its permeability, perhaps by more than an order of magnitude. Nonetheless, after about  $t = 12,300$  s, pore pressures had climbed to positive values in all tensiometers except those (22 and 25) farthest upslope. At about  $t = 13,300$  s, the data-acquisition system for the tensiometers failed. However, because pore pressures were for the most part positive at this time, we were able to extend the records for tensiometers 20, 21, 23, 24, and 26 by appending data from the adjacent dynamic-response pore-pressure transducers. This provided a complete record of pore pressures at five locations up to and during failure, as shown in Figure 17.

Extensometer data recorded prior to slope failure indicated that premonitory soil deformation substantially exceeded that in experiment I. Beginning at  $t = 13,000$  s, detectable downslope soil creep commenced. This creep did not accelerate but remained virtually constant at a rate of about 0.1 mm/s until rapid slope failure occurred at  $t = 13,776$  s. Extensometers 1 and 2 yielded nearly identical records of the pre-failure creep. Both extensometers were located downslope from a conspicuous series of tension cracks that developed in the midslope area and are visible in Figure 18D. However, the tension cracks did not accommodate all downslope displacement, which totalled nearly 70 mm. Some displacement was accommodated by distributed strain. This strain apparently involved soil dilation, as evidenced by declining pore pressures at the end of the records for tensiometers 20, 21, and 24 (Figure 17). The onset of pore-pressure decline corresponded almost exactly with the onset of measurable downslope creep. Landslide experiments reported by Iverson & LaHusen (1989) and by Harp et al (1990) showed similar evidence of pore-pressure decline preceding failure.

Slope rupture at  $t = 13,776$  s initially involved only about  $1 \text{ m}^3$  of soil and was localized on the lower right half of the slope, as seen in Figure 18E. Both extensometer anchors were displaced by this initial failure but were located in areas that did not experience the maximum acceleration. Within about 1 s of the first failure, slope rupture retrogressed into material upslope and adjacent to the

first moving block. A process of block-by-block failure continued for several seconds until eventually  $2.1 \text{ m}^3$  of soil had evacuated the slope. However, failure did not retrogress to the head of the soil prism, nor did it appear to penetrate to the base of the soil prism. The anchor of extensometer E2 remained pinned against the retaining wall at the conclusion of the experiment. The other extensometer anchor (E1) continued downslope with the debris flow until its cable pulled out.

The debris flow that mobilized in experiment II accelerated less rapidly than that in experiment I and did not achieve a liquefied appearance until after it evacuated the source area, descended the  $50^\circ$  ramp (Figure 15), and became thoroughly agitated. The bulk density of the flowing debris, estimated from flow-depth and basal normal stress measurements as described by Iverson (1997), was indistinguishable from that of the debris flow in experiment I. Water-balance data (Table 2) indicate that the experiment II debris flow probably contained about as much water as the experiment I flow. We therefore attribute the differences in flow appearance to differences in initial soil bulk density, water distribution, and mobilization mechanics. The first block of soil to fail in experiment II appeared to be relatively thin and to incorporate mostly unsaturated soil. The consequent rigidity of the block appeared to retard rapid, spontaneous mobilization of the type observed in experiment I.

Despite evidence of premonitory dilation in experiment II, Figure 17 shows that pore pressures rose sharply during slope failure, similar to the response in experiment I. Pore-pressure sensors below the water table registered pressure increases similar in magnitude to those in experiment I, indicating that  $\partial p/\partial z \sim 10\text{--}14 \text{ kPa/m}$  and that liquefaction or near-liquefaction occurred at least locally. In contrast, sensors at or above the water table (*E* and *F*) registered little or no dynamic pore-pressure response. Flashing to positive pore pressures that accompanied failure in experiment I did not occur in experiment II. TDR data indicated that volumetric water contents in the unsaturated zone at the time of failure in experiment II were as high or higher than those in experiment I. Lack of pervasive soil contraction during failure in experiment II provides the most likely explanation for the lack of pore-pressure flashing. However, contraction apparently did occur in some places, where pore pressure rose sharply. A key difference between experiments I and II may involve the degree to which contraction spread from point to point by failure-induced soil agitation. The denser soil of experiment II may have inhibited this process. Also, because the soil mass and acceleration of the initial failure in experiment I exceeded those in experiment II, greater kinetic energy was available to drive soil agitation.

The small size and largely unsaturated condition of the initial failure in experiment II not only inhibited rapid mobilization; it also raised mechanical

questions. Limit-equilibrium analysis of the initial failure using the same Janbu (1973) method as for experiment I yielded a minimum  $FS$  of 1.28 (Figure 19B). Our analysis accounted for the presence of the tension cracks observed at the upslope margin of the failed mass and for the measured distribution of pore pressures. As in Figure 19A, we obtained the pore-pressure heads in Figure 19B by numerically fitting a steady groundwater-flow solution to the pore pressures measured immediately prior to slope failure. Figure 19B shows two examples of trial slip surfaces used in the limit-equilibrium analysis. The deeper slip surface intersects the low-friction flume bed and encompasses much soil below the water table. Nonetheless, the computed  $FS$  for this slip surface is 1.45, whereas the  $FS$  for the shallower slip surface, located where we believe the initial failure occurred, is 1.28. The difference in these factors of safety illustrates the strongly two-dimensional character of the failure: In a one-dimensional (infinite-slope) analysis, the deeper failure surface would clearly have a lower  $FS$  than the shallower surface. Thus in some situations, inferences drawn from infinite-slope analysis can be seriously flawed.

The perplexing degree to which the computed limit-equilibrium  $FS$  (1.28) exceeds the theoretical value of 1.0 motivated us to consider alternative means of assessing the soil stress state that provoked failure. Static indeterminacy of two-dimensional stress fields dictates that there is no “correct” method of assessment. The elastic effective-stress analysis described by Iverson & Reid (1992), and Reid & Iverson (1992) provides an alternative to limit-equilibrium analysis. Figure 20 shows results of finite-element calculations of effective stresses using this methodology. The elastic calculations assumed the same pore-pressure distribution as that depicted in Figure 19B and a soil Young’s modulus  $E = 1.65 \times 10^7$  Pa and Poisson’s ratio  $\nu = 0.5$ . This value of  $\nu$  implies that compression in one direction is balanced by compensating expansion in the orthogonal direction, and it maximizes the lateral stress transfer in elastic calculations. This assumption seems justified for soil on the verge of Coulomb failure, wherein lateral stress transfer is great. The elastic calculations simulated the effects of the downslope retaining wall and underlying concrete flume bed by specifying that these structures were very stiff, with  $E = 9.65 \times 10^{10}$  Pa and  $\nu = 0.25$ . These values are appropriate for concrete, and they caused the computed displacements in the flume bed and retaining wall to be much smaller than those in the adjacent soil. Far from the boundaries of the soil, we specified zero-displacement boundary conditions for the retaining wall and bed. These boundary conditions affected the computed soil stresses negligibly. At the surface of the soil we specified a stress-free boundary.

Figure 20A depicts the magnitudes and directions of principal effective stresses computed using the elastic model, and Figure 20B depicts the computed distribution of Coulomb failure potential  $\Phi$ , defined by Iverson & Reid

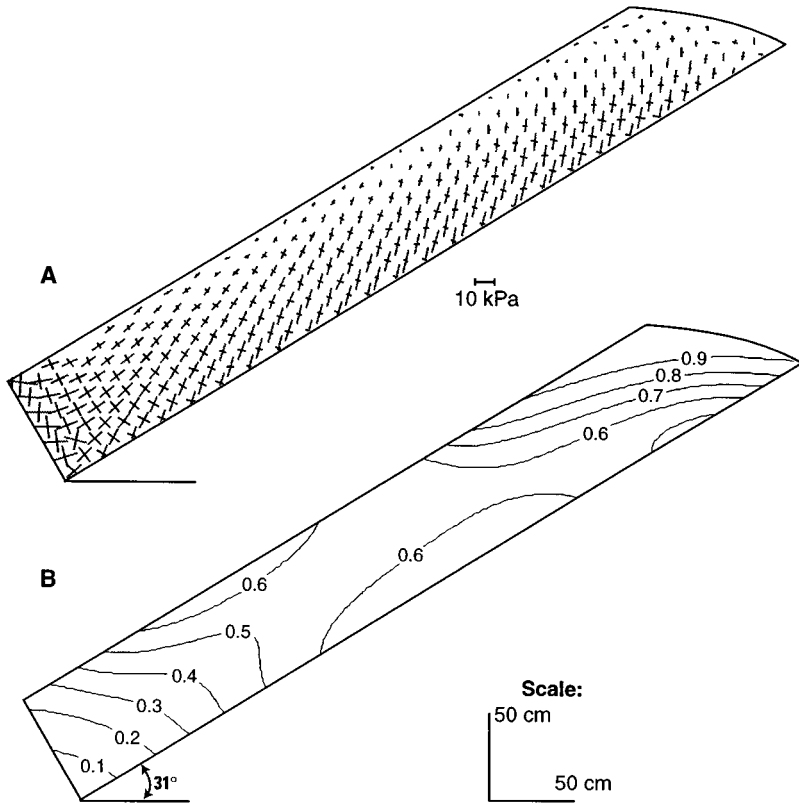


Figure 20 (A) Simulated orientation and relative magnitude of principal effective stresses in experiment II, calculated using finite-element methodology described by Iverson & Reid (1992). The calculation used the pore-pressure head distribution depicted in Figure 19B. (B) Contours of Coulomb failure potential,  $\Phi$ , calculated from the effective-stress field shown in A.

(1992) as

$$\Phi = \frac{\sigma'_1 - \sigma'_3}{\sigma'_1 + \sigma'_3} = \frac{|\tau_{\max}|}{\sigma'_{\text{mean}}}, \tag{19}$$

in which  $\sigma'_1$  and  $\sigma'_3$  are the major and minor principal effective stresses,  $\sigma'_{\text{mean}}$  is the mean effective stress, and  $\tau_{\max}$  is the maximum shear stress. The  $\Phi$  value provides a scalar index of the proximity of the local stress state to a Coulomb failure state, but it neither supposes nor delineates failure surfaces. For a cohesionless soil,  $\Phi = \sin \phi$  at failure, which yields  $\Phi = 0.64$  at failure for the soil used in experiments I and II.

Noteworthy aspects of the effective stress field shown in Figure 20A include its overall similarity to the infinite-slope stress fields shown in Figure 11 but also the degree to which stresses react to the presence of the retaining wall and free surface. Near the retaining wall,  $\sigma'_1$  rotates to a nearly slope-parallel orientation, and  $\sigma'_3$  becomes more nearly equal to  $\sigma'_1$ . Near free surfaces, effective stresses are generally small, and stress components normal to the surface are particularly small.

Figure 20B facilitates interpretation of Figure 20A by depicting contours of  $\Phi$  computed from the effective stresses. (The density of the finite-element grid used in computations was double that indicated by the spacing of symbols in Figure 20A.) The contours show that the highest failure potential theoretically existed near the apex of the slope, but this is an artifact of the tendency for elastic stresses to become nearly tensile in this region. More relevant concentrations of high failure potential ( $\Phi = 0.6$ ) exist in the midslope area, both at depth and near the surface. The near-surface region of high failure potential corresponds quite well with the locus of initial slope failure. The comparably sized region of high failure potential adjacent to the bed did not initiate failure, however, despite the relative weakness of the soil-concrete interface (Table 2). The apparent explanation for this observation is the presence of a large zone of relatively low failure potential between this weak bed region and the retaining wall downslope. A failure surface originating at the bed would have to pass through a region of comparatively great soil strength to reach the soil surface near the retaining wall.

## CONCLUSION

Field observations, laboratory experiments, and theoretical analyses indicate that landslides may mobilize to form debris flows by three processes: (a) widespread Coulomb failure within a soil mass, (b) partial or complete soil liquefaction by high pore-fluid pressures that may cause or accompany Coulomb failure, and (c) conversion of landslide translational energy to internal vibrational energy (i.e. granular temperature). These processes can operate independently, but in many circumstances they appear to operate simultaneously and synergistically. Early work on debris-flow mobilization described a similar interplay of processes but featured mechanical models that were tailored to fit the rather restrictive precepts of Bingham or Bagnold debris-flow theories (e.g. Johnson & Rahn 1970, Rodine 1974, Takahashi 1978). These mechanical models excluded pore-pressure effects that cause soil liquefaction and neglected granular temperature as a factor that influences apparent soil rigidity. In contrast, in this review we emphasize a perspective of mobilization mechanics in which liquefaction and granular temperature are crucial components (cf Iverson 1997).

Most landslides that mobilize to form subaerial debris flows are triggered by increased pore-water pressures associated with rainfall, snowmelt, or groundwater inflow from adjacent areas. If soil pore space throughout the landslide mass is saturated or nearly saturated at the time of slope failure, the potential for debris-flow mobilization is increased. Infiltration of surface water under vertical hydraulic gradients  $\partial h/\partial z \sim -1$  or growth of a capillary fringe above a water table can nearly saturate pore spaces while negative pore pressures persist. Increases in pore pressure as a result of transient groundwater perching on low-permeability layers can then trigger failure of an unsaturated but nonetheless very wet soil mass. Positive pore pressures that trigger slope failure need not liquefy the soil, but high pore pressures associated with upward components of groundwater flow enhance the potential for debris-flow mobilization.

Many of the phenomena that influence debris-flow mobilization can be quantified in a rudimentary way using infinite-slope mechanics. Infinite slopes are mathematically one-dimensional and statically determinate, which leads to unambiguous quantitative results. Significant results include the following: (a) Vertical pore-pressure gradients described by  $\partial p/\partial z = \gamma_t \cos^2 \theta$  will liquefy failing, cohesionless soils on slopes inclined at the angle  $\theta$ . Thus as slope angles steepen, vertical pore-pressure gradients necessary to liquefy the soil decline. (b) If cohesion can sustain the stability of a steep slope until it becomes saturated, the soil is apt to liquefy spontaneously if cohesion is disrupted during failure. This result can best be appreciated by considering an infinite-slope factor-of-safety ( $FS$ ) analysis that places no unnecessary constraints on pore-pressure distributions and employs nondimensional terms for frictional effects ( $T_f$ ), groundwater effects ( $T_w$ ), and cohesion effects ( $T_c$ ). The analysis shows that  $FS = T_f + T_w + T_c = 1$  applies for Coulomb failure and  $T_f + T_w = 0$  applies for liquefaction. Thus if  $T_c = 1$  at the time of failure, the soil mass will liquefy if agitation subsequently destroys the cohesive strength. (c) A simple landslide dynamics model can be used to estimate the maximum volumetric density of internal kinetic energy available to destroy cohesive bonds. This energy density is given by  $\gamma_t H (1 - FS)$ , where  $H$  is the distance of vertical descent of a steadily sliding landslide mass. This expression illustrates the potential for synergistic feedback between changes in the pore-pressure distribution (which determines  $T_w$  and thereby affects  $FS$ ) and changes in landslide descent rate and vibrational energy (granular temperature). (d) Pore-pressure changes that result from soil dilation or contraction can occur if the initial soil density differs from the critical-state density and the nondimensional hydraulic diffusivity,  $t_{def}/t_{diff}$ , is sufficiently small. Fine-grained soils are most likely to have large  $t_{diff}$ , but calculations show that loosely packed sand-and-gravel soils can have sufficiently small  $t_{def}/t_{diff}$  to produce excess pore pressures when rapid slope failure occurs.

These excess pressures add to the pore pressures that trigger failure, and during failure they enhance the potential for debris-flow mobilization.

Measurements of key mechanical quantities such as pore pressures and failure speeds during debris-flow mobilization in field settings have proven elusive, but laboratory experiments have been effective for gaining an understanding of the complicated mobilization dynamics of two-dimensional slopes. Experiments and analyses described herein illustrate that two distinct modes of mobilization are possible even when soil properties and average water contents are similar. In mode I mobilization, liquefaction is almost spontaneous. Pore pressures throughout the soil rise sharply as the soil fails, and the soil quickly attains a liquefied appearance. In regions above the pre-failure water table, pore pressures can become positive almost instantaneously. Groundwater saturation along the entire failure surface and loose soil packing both appear to enhance this process. In mode II mobilization, the initial failure is slower and more piecemeal, and may involve retrogressive slumping of multiple soil blocks. The mass may liquefy partially but not completely during the initial failure. Fully mobilized flow does not occur until the moving mass has descended some distance and become thoroughly agitated by conversion of translational energy to granular temperature. This style of mobilization appears most probable when soils are somewhat denser and slip surfaces are less completely saturated than in mode I. Field observations provide corroborating evidence of these distinctive styles of mobilization (e.g. Ellen et al 1988), but a gradation between the two styles is certainly possible.

#### ACKNOWLEDGMENTS

We thank Scott Anderson and Steve Ellen for constructive criticism that helped improve this paper. We thank Jon Major, Tony Bequette, Kevin Hadley, and Sarah Christian for assistance with experiments.

Visit the *Annual Reviews* home page at  
<http://www.annurev.org>.

## APPENDIX 1: DERIVATION OF THE PORE-PRESSURE DIFFUSION EQUATION

Relationships necessary to obtain the one-dimensional, linear, pore-pressure diffusion equation are:

- (a) a one-dimensional mass balance,  $\partial v'_y / \partial y = -\partial q_y / \partial y$ , which assumes that solid and fluid constituents are incompressible, that the solid velocity  $v'_y$

describes all deviation from  $v_x$ , and that the one-dimensional fluid specific discharge  $q_y$  is measured relative to the moving solid;

- (b) a strain-rate definition,  $\dot{\epsilon}_{yy} = \partial v'_y / \partial y$ , which assumes that strains are small;
- (c) Darcy's law for fluid specific discharge,  $q_y = -K(\partial h / \partial y)$ , which assumes a scalar value of  $K$ ;
- (d) a one-dimensional, effective-stress definition given by  $\sigma'_{yy} = \sigma_{yy} - p$ ;
- (e) a linear, one-dimensional stress-strain rule,  $\sigma'_{yy} = E\epsilon_{yy}$ , in which the stiffness  $E$  is constant;
- (f) a relation between pore pressure and hydraulic head,  $h = (p / \rho_w g) - z$ .

Combination of relationships *a*, *b*, and *c* yields an expression for the strain rate,  $\dot{\epsilon}_{yy} = -K(\partial^2 h / \partial y^2)$ ; and combination of relationships *d*, *e*, and *f*, followed by differentiation with respect to time, yields an alternative strain-rate expression,  $\dot{\epsilon}_{yy} = (-\rho_w g / E)(\partial h / \partial t)$ . Equating these two expressions for  $\dot{\epsilon}_{yy}$  yields a diffusion equation for hydraulic head,

$$\frac{\partial h}{\partial t} = \frac{KE}{\rho_w g} \frac{\partial^2 h}{\partial y^2}. \quad (\text{A1})$$

The hydraulic head consists of the sum of a steady component and deviation from steady state,  $h = h_{steady} + h'$ . The theory of partial differential equations shows that solutions of Equation A1 may be decomposed to a solution for the unsteady component  $h'$  plus a solution of  $\partial^2 h_{steady} / \partial y^2 = 0$  (e.g. Carslaw & Jaeger 1959). In this case, the solution for  $h_{steady}$  describes the ambient groundwater flow field at the time of slope failure, and the solution for  $h'$  describes the groundwater response to strain during soil deformation. Moreover, because  $h'$  lacks a hydrostatic component,  $h' = p' / (\rho_w g)$  and Equation A1 reduces to a diffusion equation for  $p'$ , as given by Equation 17.

#### Literature Cited

- Abdel-Salam A, Chrysikopoulos CV. 1996. Unsaturated flow in a quasi-three-dimensional fractured medium with spatially variable aperture. *Water Resour. Res.* 32:1531-40
- Adams MJ, Briscoe BJ. 1994. Deterministic micromechanical modeling of failure or flow in discrete planes of densely packed particle assemblies: introductory principles. In *Granular Matter*, ed. A Mehta, pp. 259-91. New York: Springer-Verlag
- Anderson MG, Burt TP. 1978. The role of topography in controlling throughflow generation. *Earth Surf. Process.* 3:331-44
- Anderson SA, Sitar N. 1995. Analysis of rainfall-induced debris flows. *J. Geotech. Eng.* 121:544-52
- Atkin RJ, Craine RE. 1976. Continuum theories of mixtures: basic theory and historical development. *Q. J. Mech. Appl. Math.* 29(2):209-44
- Atkinson JH. 1981. *Foundations and Slopes—An Introduction to Applications of Critical*

- State Soil Mechanics*. New York: Wiley. 382 pp.
- Bagnold RA. 1954. Experiments on a gravity-free dispersion of large solid spheres in a Newtonian fluid under shear. *Proc. R. Soc. London Ser. A* 225:49–63
- Baum RL, Fleming RW. 1991. Use of longitudinal strain in identifying driving and resisting elements in landslides. *Geol. Soc. Am. Bull.* 103:1121–32
- Baum RL, Reid ME. 1995. Geology, hydrology, and mechanics of a slow-moving, clay-rich landslide, Honolulu, Hawaii. In *Clay and Shale Slope Instability*, ed. WC Haneberg, SA Anderson, 10:79–105. Boulder, CO: Geol. Soc. Am. Rev. Eng. Geol.
- Bear J. 1972. *Dynamics of Fluids in Porous Media*. New York: Dover. 764 pp.
- Blake GR. 1965. Bulk density. In *Methods of Soil Analysis*, ed. CA Black, DD Evans, JL White, LE Ensminger, FE Clark, pp. 374–90. Madison, WI: Am. Soc. Agron.
- Bovis MJ, Dagg BR. 1992. Debris flow triggering by impulsive loading: mechanical modeling and case studies. *Can. Geotech. J.* 29:345–52
- Brand EW. 1981. Some thoughts on rainfall induced slope failures. *Proc. 10th Int. Conf. Soil Mech. Found. Eng.* pp. 373–76
- Buchanan P, Savigny KW, De Vries J. 1990. A method for modeling water tables at debris avalanche headscarp. *J. Hydrol.* 113:61–88
- Caine N. 1980. The rainfall intensity-duration control of shallow landslides and debris flows. *Geogr. Ann.* A62:23–27
- Campbell CS. 1990. Rapid granular flows. *Annu. Rev. Fluid Mech.* 22:57–92
- Campbell RH. 1975. Soil slips, debris flows, and rainstorms in the Santa Monica Mountains and vicinity, southern California. *US Geol. Surv. Prof. Pap.* 851. 51 pp.
- Cannon SH, Ellen S. 1985. Rainfall conditions for abundant debris avalanches, San Francisco Bay Region, California. *Calif. Geol.* 38:267–72
- Cannon SH, Savage WZ. 1988. A mass-change model for the estimation of debris-flow runout. *J. Geol.* 96:221–27
- Carlslaw HS, Jaeger JC. 1959. *Conduction of Heat in Solids*. Oxford: Oxford Univ. Press. 510 pp. 2nd ed.
- Casagrande A. 1976. Liquefaction and cyclic deformation of sands—a critical review. *Harv. Soil Mech. Ser.* 88. 51 pp.
- Costa JE, Wieczorek GF, eds. 1987. *Debris Flows/Avalanches: Process, Recognition, and Mitigation*, Vol. 7. Boulder, CO: Geol. Soc. Am. Rev. Eng. Geol.
- Coulomb CA. 1773. Sur une application des règles de maximis et minimis à quelques problèmes des statique relatifs à l'architecture. *Acad. R. Sci. Mem. Math. Phys.* 7:343–82
- de Boer R, Ehlers W. 1990. The development of the concept of effective stress. *Acta Mech.* 83:77–92
- Denlinger RP, Iverson RM. 1990. Limiting equilibrium and liquefaction potential in infinite submarine slopes. *Mar. Geotechnol.* 9:299–312
- Drake TG. 1990. Structural features in granular flows. *J. Geophys. Res.* 95(B6):8681–96
- Drake TG. 1991. Granular flow: physical experiments and their implications for microstructural theories. *J. Fluid Mech.* 225:121–52
- Eckersley D. 1990. Instrumented laboratory flowslides. *Geotechnique* 40:489–502
- Ellen SD, Albus MA, Cannon SH, Fleming RW, Lahr PC, et al. 1988. Description and mechanics of soil slip/debris flows in the storm. See Ellen & Wieczorek 1988, pp. 63–112
- Ellen SD, Fleming RW. 1987. Mobilization of debris flows from soil slips, San Francisco Bay region, California. See Costa & Wieczorek 1987, pp. 31–40
- Ellen SD, Wieczorek GF, eds. 1988. Landslides, floods, and marine effects of the storm of January 3–5, 1982, in the San Francisco Bay Region, California. *US Geol. Surv. Prof. Pap.* 1434. 310 pp.
- Fairchild LH. 1987. The importance of lahar initiation processes. See Costa & Wieczorek 1987, pp. 51–61
- Fleming RW, Ellen SD, Albus MA. 1989. Transformation of dilative and contractive landslide debris into debris flows—an example from Marin County, California. *Eng. Geol.* 27:201–23
- Fukuzono T. 1985. A new method for predicting the failure time of a slope. *Proc. 4th Int. Conf. Field Workshop Landslides*, pp. 145–50. Tokyo: Jpn. Landslide Soc.
- Gillham RW. 1984. The capillary fringe and its effect upon water-table response. *J. Hydrol.* 67:307–24
- Greenway DR. 1987. Vegetation and slope stability. In *Slope Stability*, ed. MG Anderson, KS Richards, pp. 187–230. New York: Wiley
- Harp EL, Wells WG II, Sarmiento JG. 1990. Pore pressure response during failure in soils. *Geol. Soc. Am. Bull.* 102:428–38
- Harr RD. 1977. Water flux in soil and subsoil on a steep forested slope. *J. Hydrol.* 33:37–58
- Heim A. 1932. *Bergsturz und Menschenleben*. Zurich: Fretz & Wasmuth. 218 pp.
- Heller PL. 1981. Small landslide types and controls in glacial deposits: lower Skagit River Drainage, Northern Cascade Range, Washington. *Environ. Geol.* 3:221–28
- Herkelrath WN, Hamburg SP, Murphy F. 1991. Automatic, real-time monitoring of soil moisture in a remote field area with time

- domain reflectometry. *Water Resour. Res.* 27:857–64
- Holzer TL, Youd TL, Hanks TC. 1989. Dynamics of liquefaction during the 1987 Superstition Hills, California, earthquake. *Science* 244:56–59
- Humphrey NF. 1982. Pore pressures in debris failure initiation. *State of Washington Water Research Center Rep. 45*. Pullman, WA. 169 pp.
- Hungr O. 1995. A model for the runoff analysis of rapid flow slides, debris flows, and avalanches. *Can. Geotech. J.* 32:610–23
- Hungr O, Morgan GC, Kellerhals R. 1984. Quantitative analysis of debris torrent hazards for design of remedial measures. *Can. Geotech. J.* 21:663–77
- Hutchinson JN. 1986. A sliding-consolidation model for flow slides. *Can. Geotech. J.* 23:115–26
- Iverson RM. 1980. Processes of accelerated pluvial erosion on desert hillslopes modified by vehicular traffic. *Earth Surf. Process.* 5:369–88
- Iverson RM. 1990. Groundwater flow fields in infinite slopes. *Geotechnique* 40:139–43
- Iverson RM. 1992. Sensitivity of stability analyses to groundwater data. In *Landslides. Proc. 6th Int. Symp. Landslides*, Vol. 1, ed. DH Bell, pp. 451–57. Rotterdam: Balkema
- Iverson RM. 1993. Differential equations governing slip-induced pore-pressure fluctuations in a water-saturated granular medium. *Math. Geol.* 23:1027–48
- Iverson RM. 1997. The physics of debris flows. *Rev. Geophys.* In press
- Iverson RM, Costa JE, LaHusen RG. 1992. Debris-flow flume at H.J. Andrews Experimental Forest, Oregon. *US Geol. Surv. Open-file Rep.* 92–483. 2 pp.
- Iverson RM, LaHusen RG. 1989. Dynamic pore-pressure fluctuations in rapidly shearing granular materials. *Science* 246:796–99
- Iverson RM, LaHusen RG. 1993. Friction in debris flows: inferences from large-scale flume experiments. In *Hydraulic Engineering '93. Proc. 1993 Conf. Hydraul. Div. Am. Soc. Civ. Eng.* 2:1604–9
- Iverson RM, Major JJ. 1986. Groundwater seepage vectors and the potential for hillslope failure and debris-flow mobilization. *Water Resour. Res.* 22:1543–48
- Iverson RM, Reid ME. 1992. Gravity-driven groundwater flow and slope failure potential: 1. Elastic effective-stress model. *Water Resour. Res.* 28:925–38
- Jaeger HM, Nagel SR. 1992. Physics of the granular state. *Science* 255:1523–31
- Jaeger HM, Nagel SR, Behringer RP. 1996. The physics of granular materials. *Phys. Today* 49(4):32–38
- Janbu N. 1973. Slope stability calculations. In *Embankment-Dam Engineering*, Casagrande Vol., ed. RC Hirschfield, SJ Poulos, pp. 47–86. New York: Wiley
- Jenkins JT, Savage SB. 1983. A theory for the rapid flow of identical, smooth, nearly elastic particles. *J. Fluid Mech.* 130:187–202
- Johnson AM. 1965. *A model for debris flow*. PhD thesis. Pennsylvania State Univ., State College
- Johnson AM. 1970. *Physical Processes in Geology*. San Francisco: Freeman, Cooper. 577 pp.
- Johnson AM. 1984. Debris flow. In *Slope Instability*, ed. D Brunsten, DB Prior, pp. 257–361. New York: Wiley
- Johnson AM, Rahn PH. 1970. Mobilization of debris flows. *Z. Geomorphol. Suppl.* 9:168–86
- Johnson KA, Sitar N. 1990. Hydrologic conditions leading to debris flow initiation. *Can. Geotech. J.* 27:789–801
- Kesseli JE. 1943. Disintegrating soil slips in the Coast Ranges of central California. *J. Geol.* 51:342–52
- Kirkby MJ, ed. 1978. *Hillslope Hydrology*. Chichester: Wiley. 389 pp.
- Kramer SL. 1988. Triggering of liquefaction flow slides in coastal soil deposits. *Eng. Geol.* 26:17–31
- Kytomaa HK. 1993. Liquefaction and solidification. In *Particulate Two-Phase Flow*, ed. MC Roco, pp. 861–83. Boston: Butterworth-Heinemann
- Lambe TW, Whitman RV. 1979. *Soil Mechanics*. New York: Wiley. 553 pp.
- Leach B, Herbert R. 1982. The genesis of a numerical model for the study of the hydrogeology of a steep hillside in Hong Kong. *Q. J. Eng. Geol.* 15:243–59
- Lill T. 1993. *A critical evaluation of a new method for determining the angle of internal friction for cohesionless sediments*. BS thesis. Beloit College, Beloit, WI. 37 pp.
- Lumb P. 1975. Slope failures in Hong Kong. *Q. J. Eng. Geol.* 8:31–65
- Lun CK, Savage SB, Jeffrey DJ, Chepurny N. 1984. Kinetic theories for granular flow: inelastic particles in Couette flow and slightly inelastic particles in a general flow field. *J. Fluid Mech.* 140:223–56
- Major JJ. 1996. *Experimental studies of deposition by debris flows: process, characteristics of deposits and effects of pore-fluid pressure*. PhD thesis. Univ. Wash., Seattle. 341 pp.
- Mandl G, Fernandez-Luque R. 1970. Fully developed plastic shear flow of granular materials. *Geotechnique* 20:277–307
- Mathewson CC, Keaton JR, Santi PM. 1990. Role of bedrock groundwater in the initiation of debris flows and sustained post-flow

- stream discharge. *Bull. Assoc. Eng. Geol.* 27:73–84
- McDonnell JJ. 1990. The influence of macropores on debris flow initiation. *Q. J. Eng. Geol.* 23:325–31
- McTigue DF, Jenkins JT. 1992. Channel flow of a concentrated suspension. *Advances in Micromechanics of Granular Materials*, ed. HH Shen, pp. 381–90. Amsterdam: Elsevier
- Melosh HJ. 1979. Acoustic fluidization; a new geologic process? *J. Geophys. Res.* 84:7513–20
- Melosh HJ. 1987. The mechanics of large rock avalanches. See Costa & Wieczorek 1987, pp. 41–49
- Mitchell JK. 1976. *Fundamentals of Soil Behavior*. New York: Wiley. 422 pp.
- Montgomery D, Dietrich WE, Torres R, Anderson SP, Heffner JT, et al. 1990. Hydrologic experiments in a steep unchanneled valley: 1. Experimental design and piezometric response. (Abstr.) *Eos, Trans. Am. Geophys. Union* 71(43):1342
- O'Connor JE, Hardison JH III, Costa JE. 1997. Debris flows from moraine-dammed lakes in the Three Sisters and Mt. Jefferson Wilderness Areas, Oregon. *US Geol. Surv. Water-Supply Pap.* In press
- O'Loughlin CL. 1972. A preliminary study of landslides in the coast mountains of southwestern British Columbia. In *Mountain Geomorphology*, ed. O Slaymaker, HJ McPherson, 14:101–11. *Br. Columbia Geogr. Ser.* Vancouver: Tantalus Res.
- Pak HK, Van Doorn E, Behringer RP. 1995. Effects of ambient gases on granular materials under vertical vibration. *Phys. Rev. Lett.* 74:4643–46
- Pariseau WG. 1980. A simple mechanical model for rockslides and avalanches. *Eng. Geol.* 16:111–23
- Passman SL, McTigue DF. 1986. A new approach to the effective stress principle. In *Compressibility Phenomena in Subsidence*, ed. SK Saxena, pp. 79–91. New York: Eng. Found.
- Phillip JR. 1991. Hillslope infiltration: planar slopes. *Water Resour. Res.* 27:109–17
- Pierson TC. 1983. Soil pipes and slope stability. *Q. J. Eng. Geol.* 16:1–11
- Pierson TC, Costa JE. 1987. A rheologic classification of subaerial sediment-water flows. See Costa & Wieczorek 1987, pp. 1–12
- Pierson TC, Iverson RM, Ellen SD. 1992. Spatial and temporal distribution of shallow landsliding during intense rainfall, southeastern Oahu, Hawaii. In *Landslides. Proc. 6th Int. Symp. Landslides*, Vol. 2, ed. DH Bell, pp. 1393–98. Rotterdam: Balkema
- Pierson TC, Janda RJ, Thouret JC, Borrero CA. 1990. Perturbation and melting of snow and ice by the 13 November 1985 eruption of Nevado del Ruiz, Columbia, and consequent mobilization, flow, and deposition of lahars. *J. Volcanol. Geotherm. Res.* 41:17–66
- Pierson TC, Scott KM. 1985. Downstream dilution of a lahar: transition from debris flow to hyperconcentrated streamflow. *Water Resour. Res.* 21:1511–24
- Plafker G, Erickson GE. 1978. Nevados Huascarán avalanches, Peru. In *Rockslides and Avalanches. 1: Natural Phenomena*, ed. B Voight, pp. 277–314. Amsterdam: Elsevier
- Pomeroy JS. 1980. Storm-induced debris avalanching and related phenomena in the Johnstown area, Pennsylvania, with reference to other studies in the Appalachians. *US Geol. Surv. Prof. Pap.* 1191. 24 pp.
- Reddi LN, Wu TH. 1991. Probabilistic analysis of ground-water levels in hillslope slopes. *J. Geotech. Eng.* 117:872–90
- Reid ME, Iverson RM. 1992. Gravity-driven groundwater flow and slope failure potential. 2. effects of slope morphology, material properties, and hydraulic heterogeneity. *Water Resour. Res.* 22:939–50
- Reid ME, Nielsen HP, Dreiss SJ. 1988. Hydrologic factors triggering a shallow hillslope failure. *Bull. Assoc. Eng. Geol.* 25:349–61
- Rice JR. 1975. On the stability of dilatant hardening for saturated rock masses. *J. Geophys. Res.* 80:1531–36
- Rickenmann D, Zimmermann M. 1993. The 1987 debris flows in Switzerland: documentation and analysis. *Geomorphology* 8:175–89
- Rodine JD. 1974. *Analysis of the mobilization of debris flows*. PhD thesis. Stanford Univ., Stanford, CA. 226 pp.
- Rodolfo KS, Umbal JV, Alonso RA, Remotigue MC, Paladio-Melosantos ML, et al. 1996. Two years of lahars on the western flank of Mount Pinatubo, Philippines: initiation, flow processes, deposits and attendant geomorphic and hydraulic changes. In *Fire and Mud: Eruptions and Lahars of Mount Pinatubo, Philippines*, ed. CG Newhall, RS Punongbayan, pp. 989–1013. Quezon City: Philipp. Inst. Volcanol. Seism./Seattle: Univ. Wash. Press
- Roeloffs E. 1996. Poroelastic techniques in the study of earthquake-related hydrologic phenomena. *Adv. Geophys.* 37:135–95
- Rogers MW, Selby MJ. 1980. Mechanisms of shallow translational landsliding during summer rainstorms, North Island, New Zealand. *Geogr. Ann. A* 62:11–21
- Rudnicki JW. 1984. Effects of dilatant hardening on the development of concentrated shear deformation in fissured rock masses. *J. Geophys. Res.* 89:9259–70

- Sasitharan S, Robertson PK, Sego DC, Morgenstern NR. 1993. Collapse behavior of sand. *Can. Geotech. J.* 30:569-77
- Sassa K. 1984. The mechanism starting liquefied landslides and debris flows. *Proc. 4th Int. Symp. Landslides* 2:349-54
- Sassa K. 1987. The Jizukiyama landslide and the interpretation of its long scraping motion. *Proc. 5th Int. Conf. Field Workshop Landslides*, pp. 215-23. Christchurch, NZ
- Savage SB. 1984. The mechanics of rapid granular flows. *Adv. Appl. Mech.* 24:289-366
- Savage WZ, Smith WK. 1986. A model for the plastic flow of landslides. *US Geol. Surv. Prof. Pap.* 1385. 32 pp.
- Schofield AN, Wroth CP. 1968. *Critical State Soil Mechanics*. London: McGraw-Hill. 310 pp.
- Selby MJ. 1976. Slope erosion due to extreme rainfall: a case study from New Zealand. *Geogr. Ann.* A 58:131-38
- Sidle RC, Swanston DN. 1982. Analysis of a small debris slide in coastal Alaska. *Can. Geotech. J.* 19:167-74
- Skempton AW. 1985. Residual strength of clays in landslides, folded strata and the laboratory. *Geotechnique* 35:3-18
- Skempton AW, DeLory FA. 1957. Stability of natural slopes in London Clay. *Proc. 4th Int. Conf. Soil Mech. Found. Eng.* 2:378-81
- Statham I. 1976. Debris flows on vegetated screes in the Black Mountains, Carmarthen-shire. *Earth Surf. Process.* 1:173-80
- Takahashi T. 1978. Mechanical characteristics of debris flow. *J. Hydraul. Div. Am. Soc. Civ. Eng.* 104:1153-69
- Takahashi T. 1980. Debris flow on prismatic open channel. *J. Hydraul. Div. Am. Soc. Civ. Eng.* 106:381-96
- Takahashi T. 1981. Debris flow. *Annu. Rev. Fluid Mech.* 13:57-77
- Takahashi T. 1991. *Debris Flow*. Rotterdam: Balkema. 165 pp.
- Temple PH, Rapp A. 1972. Landslides in the Mgeta area, western Uluguru Mountains, Tanzania. *Geogr. Ann.* A 54:157-93
- Terzaghi K. 1936. The shearing resistance of saturated soils and the angle between the planes of shear. *Proc. 1st Int. Conf. Soil Mech.* 1:54-56
- Vaid YP, Thomas J. 1995. Liquefaction and postliquefaction behavior of sand. *J. Geotech. Eng.* 121:163-73
- Vallance JW, Scott KM. 1996. The Osceola mudflow from Mount Rainier: sedimentology, behavior, and hazard implications of a huge cohesive debris flow. *Geol. Soc. Am. Bull.* In press
- Vallejo LE. 1979. An explanation for mudflows. *Geotechnique* 29:351-53
- Van Gassen W, Cruden DM. 1989. Momentum transfer and the friction in the debris of rock avalanches. *Can. Geotech. J.* 26:623-28
- Varnes DJ. 1978. Slope movement types and processes. In *Landslides—Analysis and Control, Transportation Res. Board Special Rep. 176*, ed. RL Schuster, RJ Krizek, pp. 11-33. Washington, DC: Natl. Acad. Sci.
- Vaughan PR, Kwan CW. 1984. Weathering, structure and in-situ stress in residual soils. *Geotechnique* 34:43-59
- Voight B. 1989. A relation to describe rate-dependent material failure. *Science* 243:200-3
- Walton O. 1993. Numerical simulation of inelastic, frictional particle-particle interactions. In *Particulate Two-Phase Flow*, ed. MC Roco, pp. 884-911. Boston: Butterworth-Heinemann
- Weyman DR. 1973. Measurements of the downslope flow of water in a soil. *J. Hydrol.* 20:267-88
- Wilson CJ, Dietrich WE. 1987. The contribution of bedrock groundwater flow to storm runoff and high pore pressure development in hollows. In *Erosion and Sedimentation in the Pacific Rim*, ed. RL Beschta, T Blinn, GE Grant, GG Ice, FJ Swanson, pp. 49-59. Publ. 162. Int. Assoc. Hydrol. Sci. Publ.
- Wilson RC, Wieczorek GF. 1995. Rainfall thresholds for the initiation of debris flows at La Honda, California. *Environ. Eng. Geosci.* 1:11-27
- Youd TL. 1973. Liquefaction, flow and associated ground failure. *US Geol. Surv. Circ.* 688. 12 pp.
- Zaslavsky D, Sinai G. 1981. Surface hydrology: parts I-V. *J. Hydraul. Div. Am. Soc. Civ. Eng.* 107:1-93
- Zhang Y, Campbell CS. 1992. The interface between fluid-like and solid-like behaviour in two-dimensional granular flows. *J. Fluid Mech.* 237:541-68
- Ziemer RR. 1981. Roots and the stability of forested slopes. In *Erosion and Sediment Transport in Pacific Rim Steeplands*, ed. TRH Davies, A Pearce, pp. 343-61. Publ. 132. Int. Assoc. Hydrol. Sci. Publ.